Quantification of peroxynitric acid and peroxyacyl nitrates using an ethane-based thermal dissociation peroxy radical chemical amplification cavity ring-down spectrometer

Youssef M. Taha[1], Matthew T. Saowapon[1], Faisal V. Assad[1], Connie Z. Ye[1], Xining Chen[1,a], Natasha M. Garner[1], and Hans D. Osthoff[1]

[1] Department of Chemistry, University of Calgary, 2500 University Drive N.W., Calgary, Alberta, Canada T2N 1N4
[a] now at: Department of Chemistry, McGill University, 801 Sherbrooke St. West, Montreal, Quebec, Canada H3A 2K6

Correspondence to: Hans D. Osthoff (hosthoff@ucalgary.ca)

Abstract. Peroxy and peroxyacyl nitrates (PNs and PANs) are important trace gas constituents of the troposphere which are challenging to quantify by differential thermal dissociation with NO_2 detection in polluted (i.e., high-NO_x) environments. In this paper, a thermal dissociation peroxy radical chemical amplification cavity ring-down spectrometer (TD-PERCA-CRDS) for sensitive and selective quantification of total peroxynitrates ($\Sigma PN = \Sigma RO_2NO_2$) and of total peroxyacyl nitrates ($\Sigma PAN = \Sigma RC(O)O_2NO_2$) is described. The instrument features multiple detection channels to monitor the NO_2 background and the RO_x (= $HO_2 + RO_2 + \Sigma RO_2$) radicals generated by TD of ΣPN and/or ΣPAN. Chemical amplification is achieved through addition of 0.6 ppm NO and 1.6% C_2H_6 to the inlet. The instrument's performance was evaluated using peroxynitric acid (PNA) and peroxyacetic or peroxypropionic nitric anhydride (PAN or PPN) as representative examples of ΣPN and ΣPAN, respectively, whose abundances were verified by iodide chemical ionization mass spectrometry (CIMS). The amplification factor or chain length increases with temperature up to 69±5 and decreases with analyte concentration and relative humidity (RH). At inlet temperatures above 120 °C and 250 °C, respectively, PNA and ΣPAN fully dissociated, though their TD profiles partially overlap. Furthermore, interference from ozone (O_3) was observed at temperatures above 150 °C, rationalized by its partial dissociation to O atoms which react with C_2H_6 to form C_2H_5 and OH radicals. Quantification of PNA and ΣPAN in laboratory-generated mixtures containing O_3 was achieved by simultaneously monitoring the TD-PERCA responses in multiple parallel CRDS channels set to different temperatures in the 60 °C to 130 °C range. The (1 s, 2 σ) limit of detection (LOD) of TD-PERCA-CRDS is 6.8 pptv for PNA and 2.6 pptv for ΣPAN and significantly lower than TD-CRDS without chemical amplification. The feasibility of TD-PERCA-CRDS for ambient air measurements is discussed.

1 Introduction

The RO_x (= $OH + HO_2 + \Sigma RO_2$) radicals and the nitrogen oxides ($NO_x = NO + NO_2$) are important trace constituents of the atmosphere that drive diverse processes such as the photochemical production of ozone (O_3) in the troposphere (Kirchner and Stockwell, 1996; Fleming et al., 2006), the catalytic destruction of O_3 in the stratosphere (Bates and Nicolet, 1950; Stenke and Grewe, 2005; Solomon, 1999; Portmann et al., 1999), and the chemistry of organic aerosol formation (Ziemann and Atkinson, 2012; Ehn et al., 2014; Crounse et al., 2013). In the troposphere, the concentrations of these species are frequently buffered by RO_x and NO_x reservoir species, of which peroxynitric acid (PNA, HO_2NO_2), alkyl peroxy nitrates such as methyl peroxynitrate ($CH_3O_2NO_2$, MPN), and the peroxyacyl nitrates (PANs, $RC(O)O_2NO_2$) are important examples (Singh et al., 1992; Roberts, 1990). Much insight into RO_x and NO_x chemistry has been gained by measuring the atmospheric abundances of these reservoirs. Significant PNA concentrations, for example, have been observed in the polar regions (Slusher et al., 2001; Davis et al., 2004; Jones et al., 2014), aloft in the free and upper troposphere (Kim et al., 2007; Murphy et al., 2004), in highly polluted environments such as the Uintah basin in winter (Veres et al., 2015), and in urban atmospheres (Spencer et al., 2009; Chen et al., 2017a), and have given valuable insights into radical budgets at these locations. The PANs and PNA are prone to thermal dissociation, such that higher concentrations are more commonly observed in cold regions, aloft in the free / upper troposphere, or in winter (Table 1). On the other hand, their rate of production is greater in summer as the actinic flux intensifies. Mixing ratios of PNA peak in the range from tens to a few hundreds of parts-per-trillion by volume (pptv, 10^{-12}) and those of peroxyacetic nitric anhydride (PAN; $CH_3C(O)O_2NO_2$) can exceed ten parts-per-billion by volume (ppbv, 10^{-9}) (Tuazon et al., 1981).

There is ongoing interest to develop improved techniques for quantification of PANs (Roberts, 2007; Wooldridge et al., 2010; Zheng et al., 2011; Tokarek et al., 2014) and PNA (Murphy et al., 2004; Spencer et al., 2009; Veres et al., 2015; Chen et al., 2017a). Thermal dissociation (TD) methods (Table 2) such as TD coupled to laser-induced fluorescence (TD-LIF) (Wooldridge et al., 2010; Day et al., 2002; Di Carlo et al., 2013), to cavity ring-down spectroscopy (TD-CRDS) (Paul et al., 2009; Thaler et al., 2011; Paul and Osthoff, 2010; Thieser et al., 2016; Sobanski et al., 2016; Womack et al., 2017), or to cavity phase-shift spectroscopy (TD-CAPS) (Sadanaga et al., 2016) detection of NO_2 are attractive as they can be used to monitor all components of odd nitrogen (NO_y) in parallel, including NO_2 (inlet operated at ambient temperature), total peroxy nitrates ($\Sigma PN = PNA + MPN + ...$; inlet heated to ~100 °C), total peroxyacyl nitrates ($\Sigma PAN = PAN +$ peroxypropinoic nitric anhydride ($C_2H_5C(O)O_2NO_2 + ...$; ~ 250 °C), total alkyl nitrates + $ClNO_2$ (ΣAN; ~ 420 °C), and HNO_3 (~ 600 °C), simply by deploying multiple detection channels and setting appropriate inlet temperatures. Molecules such as NO and HONO can be quantified through addition of O_3 following TD (Wild et al., 2014; Womack et al., 2017; Fuchs et al., 2009). When used in polluted (i.e., high-NO_x) environments, however, a drawback of the TD methods is that quantification of ΣPN (and, to a lesser degree, also of ΣPAN) is compromised because of the large error introduced from subtraction of the NO_2 background, which is often 2 – 4 orders of magnitudes larger than the ΣPN abundance. In such high-NO_x environments, on the other hand, mixing ratios of RO_x radicals are generally much smaller, < 100 pptv (Wood et al., 2016), than those of NO_2, such that a better strategy may be to quantify the peroxy and peroxyacyl radicals generated in stoichiometric amounts during TD of ΣPN and/or ΣPAN rather than NO_2.

The RO_x radicals may be quantified by chemical ionization mass spectrometry (CIMS) (Hanke et al., 2002; Edwards et al., 2003; Chen et al., 2004; Slusher et al., 2004; Hornbrook et al., 2011); in fact, a TD-CIMS method has been developed to quantify PAN by titrating the peroxyacetyl radical with iodide reagent ion (Slusher et al., 2004). Other RO_x radical detection methods include LIF (Faloona et al., 2004; Heard, 2006; Fuchs et al., 2008; Dusanter et al., 2009) and peroxy radical chemical amplification (PERCA) coupled to NO_2 detection (Cantrell et al., 1984; Hastie et al., 1991; Green et al., 2006; Liu and Zhang, 2014; Horstjann et al., 2014). The PERCA method is attractive as it allows the infrastructure of existing TD instruments with NO_2 detection to be utilized.

In PERCA coupled to NO_2 detection, concentrations of RO_x radicals are amplified by factors of between ~20 to ~190 through a series of catalytic reactions, usually involving parts-per-million by volume (ppmv, 10^{-6}) mixing ratios of nitric oxide (NO) and percent levels of either carbon monoxide (CO) (Cantrell et al., 1984) or a short chain hydrocarbon such as ethane (C_2H_6) (Mihele and Hastie, 2000; Wood et al., 2016) (R1-R6, Table 3). Under these conditions, the peroxy radicals catalytically convert NO to NO_2, and the amount of NO_2 produced over a constant reaction period is proportional to the number of radicals that were present originally.

The measurement of peroxy radicals by PERCA is prone to matrix effects and interferences. For instance, a key operational parameter of any PERCA instrument is the radical chain length or amplification factor (CL), which must be carefully calibrated. This chain length is suppressed by water vapour, whose presence increases the rates of radical loss on the inner walls of the PERCA chamber and the rates of certain gas-phase reactions, e.g., the reaction between the hydroperoxyl radical - water dimer ($HO_2 \cdot H_2O$) with NO to peroxynitrous acid (HOONO) which isomerizes to nitric acid ($HONO_2$) (Mihele and Hastie, 1998; Mihele et al., 1999 ; Mihele and Hastie, 2000). The most obvious way to minimize wall reactions and to prevent weakly bound clusters such as $HO_2 \cdot H_2O$ from forming is to apply heat. When quantification of ambient RO_x radicals is the goal, this is avoided to prevent TD of ΣPN or ΣPAN (which are more abundant than free RO_x radicals). TD of ΣPN or ΣPAN produces radicals that interfere with the measurement of free RO_x radicals (Mihele and Hastie, 2000). On the other hand, if measurement of ΣPN or ΣPAN is desired (such as in this paper), this interference is turned into a measurement principle. We are aware of only one prior attempt to quantify peroxy nitrates in this manner: Blanchard et al. thermally decomposed PAN eluting from a chromatographic column in the presence of NO and CO and quantified the amplified NO_2 using luminol chemiluminescence (Blanchard et al., 1993).

In this manuscript, we probe the feasibility of selectively quantifying ΣPN and ΣPAN through their respective peroxy radical TD fragments by thermal decomposition peroxy radical chemical amplification cavity ring-down spectroscopy (TD-PERCA-CRDS). The instrument uses a 405 nm blue diode laser CRDS (Paul and Osthoff, 2010) to monitor NO_2 and the ethane-based chemical amplification scheme described by Wood et al. (2016), chosen because of ethane's lower toxicity compared to CO. Thermal dissociation profiles were determined for PAN, PPN, and PNA. Quantification of trace levels of PAN, PPN, and PNA by TD-PERCA-CRDS is demonstrated and compared to parallel measurements by iodide CIMS. The suitability of TD-PERCA-CRDS as a highly sensitive (sub-pptv) ΣPN and ΣPAN detection method for ambient measurements is discussed.

2 Experimental Section

2.1 TD-PERCA-CRDS

2.1.1 Single-channel inlet

The majority of the experiments described in this manuscript were conducted using a single-channel TD-PERCA inlet that is described and depicted as Figure S1 of the Electronic Supplementary Material of (Taha et al., 2018). Briefly, NO in N_2 (100.2 ppmv, Scott-Marrin, Riverside, CA) was scrubbed of NO_2 by passing through iron(II) sulfate heptahydrate (99%, Sigma-Aldrich, Oakville, ON) prior to being combined with either a flow of N_2 gas (Praxair) or ethane (CP grade, 99%, Matheson, Baskin Ridge, NJ). The gas mixture was directed towards the 80-cm long PERCA chamber (1.27 cm or ½" outer diameter (o.d.)). When NO and N_2 were mixed prior to the PERCA chamber, a "PERCA off" signal was observed, and ethane was added after the PERCA chamber to maintain constant flow (and pressure) through the system. Conversely, when NO and ethane were directed towards the PERCA chamber a "PERCA on" signal was observed. To maintain flows and pressures through the system during "PERCA on" mode, N_2 was added to the inlet at an addition point after the PERCA chamber.

The inlet was connected to a four-channel CRDS described elsewhere (Odame-Ankrah, 2015). Briefly, concentrations of NO_2 were monitored via its absorption at 405 nm (Paul and Osthoff, 2010). A flow containing ppmv levels of O_3 in O_2 was added to one CRDS channel to monitor NO_x (Fuchs et al., 2009). The remaining two channels were equipped with heated quartz tubes to monitor NO_2 + ΣPAN and NO_2 + ΣPAN + total alkyl nitrates

(ΣAN) (Paul et al., 2009). Each channel was connected to a MFC set to a flow rate of ~0.84 slpm. All four CRDS cells were connected to sample the gases exiting the single-channel TD-PERCA inlet, though in principle a single CRDS detection channel would have sufficed to carry out the measurements.

When radical free "zero" air was sampled with the single channel inlet, a negative offset (up to 1 ppbv) was observed when the 3-way solenoid valves were switched between PERCA "on" and "off" (data not shown). This artefact was not observed with the dual channel setup (section 2.1.2) and was not further investigated but may have been caused by differences in the ethane flows through the needle valve induced by pressure changes (up to 15 Torr) during switching between PERCA on and off.

2.1.2 Dual-channel TD-PERCA-CRDS

Time resolution, signal-to-noise, and subtraction of background NO_2 can be significantly improved in a PERCA instrument by implementing dual detection channels where both amplified and background signals are simultaneously monitored (Green et al., 2006; Cantrell et al., 1996). The dual channel TD-PERCA setup used in this work is shown in Figure 1. The NO reagent gas is added at the same flow rate and concentration as in the single-channel version near the tip of the inlet (after the zero air and calibration gas ports). The residence time prior to the ethane addition point (~2.0 s) suffices to destroy RO_x radicals (via reaction with NO) prior to chemical amplification. Addition of either NO or ethane is on/off modulated using 2-way normally-open valves connected to a pump via 50 μm critical orifices (Lenox Laser, Glen Arm, MD) in a similar fashion as described earlier (Odame-Ankrah and Osthoff, 2011).

A portion of the sample flow of ~0.74 slpm was diverted prior to TD to monitor the "background" NO_2 concentration in one CRDS channel. The remaining flow (~2.2 slpm) was passed through the heated quartz tube and PERCA chamber as described earlier and sampled by the other three CRDS channels to monitor background NO_2 plus the amplified NO_2 signal.

2.1.3 Four-channel differential temperature TD-PERCA-CRDS

An instrument with four identical measurement channels was set up to enable simultaneous quantification of NO_2, NO_2 + ΣPN and NO_2 + ΣPN + ΣPAN. This version was similar to dual channel setup described above and simply added two additional PERCA chambers; all three PERCA chambers were connected to separate CRDS channels. The quartz PERCA chamber was replaced with three identical 1.27 cm (1/2") o.d. and 0.95 cm (3/8") i.d. fluorinated ethylene propylene (FEP) Teflon™ tubes externally heated using stretch-to-fit heaters (Watlow, St. Louis, MO) to 60, 80 and 100 °C, respectively. A common inlet filter was placed between the PERCA chambers and the ethane addition point. A flow restriction was placed ahead of the common filter to achieve a pressure of 380 - 400 Torr at a flow rate of 0.8 slpm per channel (total flow rate ~3.2 slpm).

2.2 Synthesis and delivery of PAN and PPN

The synthesis of PAN and PPN from their corresponding anhydrides was described earlier (Mielke and Osthoff, 2012; Furgeson et al., 2011). Aliquots in tridecane were stored in 2.0 mL centrifuge tubes (VWR) in a freezer until needed.

To separate PAN and PPN from impurities generated during synthesis and storage (i.e., NO_2, HNO_3 and alkyl nitrates (Grosjean et al., 1994)), a preparatory scale GC setup (Figure 2) was used. First, the contents of two tubes containing PAN and PPN in tridecane were combined in a 3-valve glass vessel. This vessel was connected to a 2-position GC-Valve (VICI Valco EH4C10WE, Houston, TX) and mildly pressurized (~0.1 atm above ambient) using oxygen (Praxair) delivered through a 10 µm critical orifice. Two megabore capillary gas chromatography (GC) columns (Restek RTX-1701, 0.53 mm i.d., 1.00 µm film thickness, State College, PA) of equal lengths (3 m) were connected to the ports adjacent to the one connected to the glass vessel. The outlet of one GC column was connected to the PERCA inlet, whereas the other was exhausted into a waste line. The port opposite to the glass vessel was also pressurized with oxygen such that both columns remained under flow at all times. Gases were delivered by switching the valve to position A (Figure 2) for ~40 s. The output of the preparatory-scale GC was diluted with ZA or air passed through a custom-built scrubber system to meet the sample flow requirements of the TD-PERCA CRDS and/or CIMS. The relative humidity (RH) of the gases delivered was monitored using a temperature/RH probe (VWR) placed inline.

The preparatory scale GC setup allowed delivery of short "bursts" of PAN and PPN. To deliver a constant and low PAN concentration over prolonged time periods, air was drawn from a 4,000 L Teflon chamber, initially filled with scrubbed (i.e., PAN-free) air and to which the head space above a PAN/tridecane solution had been added. An internal mixing fan ensured constant output.

2.3 Synthesis and delivery of PNA

2.3.1. Batch sample

A batch PNA sample was synthesized from reaction of nitronium tetrafluoroborate (NO_2BF_4; Sigma-Aldrich) with H_2O_2 as described by Chen et al. (2017a). Briefly, a 50% H_2O_2 solution (Sigma-Aldrich) was concentrated using a gentle N_2 flow over a period of several days. A small aliquot (200 µL) of concentrated H_2O_2 was placed in a 3-valve glass vessel cooled to 0 °C using an external circulating chiller, and 120 mg of NO_2BF_4 were added. The headspace of the glass vessel was flushed with a 50 sccm flow of N_2 delivered by a MFC. This flow delivered very high concentrations and contained substantial and variable amounts of impurities (mainly HNO_3), even when the vessel temperature was lowered to -20 °C. The batch sample was used to calibrate the CIMS against TD-CRDS (section 2.4).

2.3.2. Photolysis source

Gas flows containing low and reproducible concentrations of PNA were generated dynamically in a similar fashion to the method described by Veres et al. (2015) by combining the output of a HO_2 photochemical source with NO_2. Ultrapure N_2 (Praxair) was passed through a bubbler filled with deionized water at a flow rate of 100 sccm and combined with 2 sccm of O_2 (Praxair). This mixture was passed through a ¼" (0.635 cm) o.d. quartz tube partially illuminated by a low-pressure 185 nm mercury quartz lamp (Jelight 95-2100-2, Irvine, CA). This generated a mixture of O_3 (~30 ppbv after dilution), OH and HO_2, whose concentrations were controlled with a sliding metal sleeve (VWR) which modified the length of the quartz tubing that was illuminated. This flow was combined with between 4 and 16 ppmv NO_2 to yield a gas mixture containing PNA which was immediately (< 5 cm tube length) diluted with zero or scrubbed air flowing at a rate slightly greater than the amount sampled by the instruments. The NO_2 gas stream was generated by mixing between 1.4 and 3.0 sccm of NO (100.2 ppmv in N_2; Scott-Marrin, Riverside, CA) with a slightly less than stoichiometric amount of O_3 in ~20 sccm O_2, generated by illuminating O_2 with a low-pressure 254 nm mercury quartz lamp (Jelight). The amount of PNA delivered from this source was quantified by TD-CRDS.

2.4 Chemical ionization mass spectrometry

The CIMS and its operation have been described elsewhere (Mielke et al., 2011; Mielke and Osthoff, 2012; Abida et al., 2011). For measurements of PAN or PPN, the instrument was operated with iodide reagent in declustering mode (collisional dissociation chamber voltage = -24.7 V) and sampled through a short section of 1.27 cm (½") o.d. PFA Teflon™ tubing heated to 190 °C. The inlet flow was diluted with nitrogen saturated with water vapour to maintain a minimum RH of ~16% with the ion-molecule reaction region (IMR). PAN and PPN were quantified using the acetate and propionate ions (*m/z* 59 and 73). Ion counts were normalized to 10^6 reagent ion counts prior to presentation. The instrument response factor for PAN was calibrated against TD-CRDS (Mielke and Osthoff, 2012) and was 11±3 Hz $pptv^{-1}$.

For PNA measurements, the CIMS was operated with an ambient temperature inlet and in clustering mode (collisional dissociation chamber voltage = -8.9 V); under these conditions, $\sim 5\times10^5$ I^- and $\sim 2\times10^4$ $I^-\cdot H_2O$ ions were observed. Mixing ratios of PNA were monitored primarily using NO_3^- at *m/z* 62, which is formed via PNA decomposition within the IMR (Abida et al., 2011). The $HNO_3\cdot I^-$ and $HO_2NO_2\cdot I^-$ clusters at *m/z* 190 and *m/z* 206 (Veres et al., 2015; Chen et al., 2017a) were also monitored.

The PNA response factors were determined using TD-CRDS (i.e., without added PERCA gases) with its inlet operated at 120 °C (Figure 3). Assuming that one equivalent of NO_2 is generated for each PNA molecule thermally dissociated, the CIMS response factors, normalized to 10^6 I^- counts, were 34.7±0.2 Hz pptv^{-1} and 0.023±0.002 Hz pptv^{-1} at *m/z* 62 and 206, respectively. These response factors are consistent with calibration factors by other groups (Veres et al., 2015; Chen et al., 2017a), with the low response at *m/z* 206 rationalized by the low number of $I^-\cdot H_2O$ ions. Even though the CIMS response at *m/z* 62 is not specific (Abida et al., 2011), it was used in the laboratory experiments presented here to monitor PNA rather than *m/z* 206 because of its larger response factor and thus higher sensitivity.

2.5 Box model simulations

Box model simulations were carried out using a subset of the MCM V3.3.1 obtained from http://mcm.leeds.ac.uk/MCM (Jenkin et al., 1997; Saunders et al., 2003; Jenkin et al., 2012) and the Kinetic Preprocessor (KPP) (Sandu and Sander, 2006) to aid in the interpretation of observations. Details are given in the S.I.

3 Results

3.1 Thermal dissociation profiles

The TD profiles of PNA, PAN, and PPN were measured by TD-CRDS (i.e., without amplification) with the single-channel inlet and are shown in Figure 4. The superimposed trend lines are simulations based on the TD model introduced by Paul et al. (2009) and the Arrhenius parameters in Table 4 and are consistent with the observations. The TD profiles of PNA and PAN/PPN partially overlap and are consistent with the 5%/95% ranges given in Figure 3 of Wooldridge et al. (2010). PNA and PAN or PPN fully dissociated at temperatures of 120 °C and 250 °C, respectively. These temperatures were used in subsequent experiments when complete dissociation of either PNA or PAN/PPN was desired. Also shown in Figure 4 is the TD-PERCA-CRDS signal observed when sampling O_3, an interfering species (see section 3.6.1).

3.2 Measurement of PAN and PPN by TD-PERCA-CRDS

A time series demonstrating amplification of PAN and PPN in the TD-PERCA-CRDS is shown in Figure 5. In this experiment, PAN and PPN were delivered via the preparatory-scale GC (Figure 2), and the single-channel setup (section 2.1.1) was used.

PAN and PPN eluted from the GC column after 3 min and 6 min, respectively. The compounds eluted as plateaus because of the relatively long (~30 s) injection time. In Figure 5A, PAN and PPN are observed only by the heated (NO_2+ ΣPAN) TD-CRDS channel. This channel was operated with its quartz inlet at 250 °C to quantitatively (see Figure 5 of (Paul et al., 2009)) decompose PAN and PPN to NO_2. In this example, mixing ratios of 2.00±0.09 ppbv and 1.86±0.12 ppbv were observed, respectively (errors are 1 σ of 1 s data). After the PERCA heater was set to 250 °C as well, similar amounts of NO_2, 2.04±0.09 ppbv and 1.97±0.12 ppbv, were observed in the ambient temperature channel for PAN and PPN, respectively. Marginally higher amounts were observed in the heated CRDS channel (2.42±0.10 and 2.06±0.14 ppbv) (Figure 5B). The lower amounts observed in the unheated CRDS channel result from recombination of peroxyacyl radicals with NO_2 (mostly in the unheated PERCA chamber), which suppresses the signal in the unheated CRDS channel but not in the heated one. Hence, the NO_2 + ΣPAN data are a more accurate measure of the PAN and PPN concentrations delivered.

Because PAN and PPN dissociate with 1:1 stoichiometry, the amount of peroxyacyl radicals produced during thermal dissociation is the same as the amount of NO_2 generated. When ~0.75 ppmv of NO was added (Figure 5C), the peroxyacyl and, subsequently, the methyl (or ethyl) peroxy, and the hydroperoxyl radicals oxidize NO to NO_2 (reactions R8/R10, R1/R5, and R3; Table 3) and the NO_2 signal relative to the signal obtained in the absence of NO is amplified by a factor of four. The ratios observed (Figure 5C relative to Figure 5B) were 4.0±0.2 and 3.8±0.3 for PAN and PPN, respectively, and are consistent with earlier observations at lower NO mixing ratios (i.e., Figure 6 of Paul and Osthoff (2010)).

Next, NO and ethane were added at mixing ratios (0.75 ppmv NO and 1.5% C_2H_6) that Wood et al. (2016) determined to be optimal for ambient temperature PERCA. Under these conditions, the signals amplified to 116.0±1.3 ppbv and 109.3±0.7 ppbv (Figure 5D), corresponding to CLs (relative to Figure 4B) of 48±2 and 53±4 for PAN and PPN, respectively.

In the presence of ethane, marginally lower NO_2 concentrations (98.7% and 98.1%) were observed in the heated, NO_2 + ΣPAN TD-CRDS channel (compared to the absence of ethane). Partial scrubbing of NO_2 in heated quartz cells has been anecdotally observed in our group's and also others' (Womack et al., 2016) TD instruments; this effect varies between quartz cells and with sample history. Since the effect was relatively minor, it was neglected in this work.

3.3 Optimization of TD-PERCA amplification factors

Sequences, such as the one shown in Figure 5, were used to determine conditions leading to optimum amplification factors. The largest amplification factors were obtained with an ethane mixing ratio of ~1.6% - 1.7% (data not shown).

Figure 6 shows how the chain length varies with NO mixing ratio. In the absence of ethane, amplification factors of ~4 were observed (Figure 6, open symbols), consistent with the results shown in Figure 5C. When 1.7% ethane were added, the amplification factor increased with NO mixing ratio up to a maximum at 550±150 ppbv and then decreased, qualitatively consistent with the results reported by Wood et al. (2016).

The amplification factors shown in Figure 6 were slightly larger for PAN than for PPN mainly because the PPN mixing ratio of ~1.3 ppbv exceeded the optimum concentration range for PERCA (see section 3.5.2).

3.4 Parallel measurement of PNA by TD-PERCA-CRDS and CIMS

A sample time series showing TD-PERCA-CRDS measurements of photochemically generated PNA in scrubbed air is presented in Figure 7. Here, the TD-PERCA-CRDS was operated with the dual channel inlet (Figure 1) at 120 °C and with 1.6% C_2H_6 and 316±3 ppbv of NO (suboptimal NO mixing ratios). Figure 7A shows the NO_2 mixing ratios in the reference, NO_2 channel (green trace) and in the TD-PERCA-CRDS channel (grey trace). In this example, the mixing ratio of PNA was changed approximately every 2 min by moving a sliding cover within the photochemical source.

The difference between these two signals is displayed in Figure 7B (red trace, left-hand axis). Superimposed in Figure 7B (right-hand axis) are the CIMS responses at *m/z* 62 (NO_3^-), *m/z* 206 ($HNO_4 \cdot I^-$, multiplied by a factor of 100 for clarity), and *m/z* 190 ($HNO_3 \cdot I^-$).

The photochemical source co-generates OH which is lost on the inner walls of the quartz tubing or is titrated by NO_2 or NO to HNO_3 or HONO, respectively. Conceivably, the co-generation of HNO_3 could interfere with quantification of PNA by CIMS at *m/z* 62. However, when the photolysis source was turned off at ~19:59 (Figure 7), HNO_3 was still observed for some time after at *m/z* 190 due to slow desorption from the inner walls of the connecting tubing, whereas the ion counts at *m/z* 62 quickly (< 10 s) returned to background values close to zero Hz, indicating that the contribution of HNO_3 to ion counts at *m/z* 62 was negligible.

The scatter plot of the TD-PERCA-CRDS and CIMS data at *m/z* 62, multiplied by the CIMS response factor determined in Figure 3A, is shown in Figure 8A as dark blue circles. The signals by the two instruments are highly correlated ($r^2 = 0.979$), consistent with both instruments measuring the same molecule, PNA. The slope of this plot (26.3±0.4) equals to the TD-PERCA-CRDS amplification factor for PNA. In contrast, the scatter plot of TD-PERCA-CRDS with the CIMS response at *m/z* 206 was unusable because of the latter's poor signal to noise ratio (Figure 3B).

3.5 Factors affecting amplification factors

The amplification factor for PNA shown in Figure 8A is less than observed for PAN in Figure 8B and for PAN and PPN under optimal conditions (Figure 6). Though in this particular example the lower amplification factor was due to the less than optimal amount of NO added, lower amplification factors for PNA than for PAN were generally observed, even when optimum NO mixing ratios were used.

The obvious difference is that different radicals, HO_2 in the case of PNA and a peroxyacyl radical ($RC(O)O_2$) in the case of PAN or PPN, are generated initially. However, in both cases, the HO_2/HO radical pair is the main carrier of the amplification, such that this initial difference should only have a marginal effect. Wood et al. (2016) estimated the uncertainty arising from the range in peroxy radical reactivity to ±9%.

Experimental parameters that can affect the amplification factor include relative humidity, radical concentration, and the PERCA inlet temperature; these factors are probed separately in the following sections. In each case, box model simulations were carried out (see S.I.) to aid in the interpretation of the data.

3.5.1 Dependence of chain lengths on relative humidity

We repeated the experiment described in section 3.4 with the scrubbed air humidified to 75% RH by passing the make-up air through a bubbler. The resulting scatter plot is superimposed in Figure 8A as red squares. Indeed, the amplification factor for PNA was lowered from 26.3±0.4 to 18.0±0.2 when the RH was increased from 20% to 75%. Following these observations, the RH dependence was investigated systematically at constant NO and ethane concentrations . The results are summarized in Figure 9.

The amplification factor decreased by (2.0±0.6)% for every 10% increase in RH. This RH dependence is less than reported for ambient temperature PERCA: Between a RH of 0% and 50%, for example, the response of room temperature PERCA dropped by 30% (Wood et al., 2016), whereas that of TD-PERCA decreased by 15%. A reduced RH dependence is expected as the elevated temperature suppresses formation of $HO_2 \cdot H_2O$ (Kanno et al., 2006), whose reaction with NO is a major radical sink (Mihele and Hastie, 1998; Mihele et al., 1999 ; Mihele and

Hastie, 2000). This interpretation is supported by box model simulations, which show a reduced RH dependence of the CL at higher temperatures (Figure S-4). In addition, we speculate that reactions of radicals on the inner walls of PERCA tubing are reduced at higher inlet temperature.

3.5.2 Dependence of chain lengths on radical concentration: dynamic range

It is well known in the PERCA community that the chain lengths decrease at high radical concentrations due to radical-radical reactions. Figures 8A and 8B demonstrate that the response of TD-PERCA-CRDS is linear for both PNA and PAN/PPN at low, atmospherically relevant mixing ratios (i.e., below ~600 pptv). The linear dynamic range is similar for PNA and PAN and PPN since the radical chain carriers are the same for both.

Figure 10 summarizes the PERCA responses as functions at larger PAN/PPN mixing ratios. The largest amplification factor, 69±5, was observed when the TD-PERCA inlet was operated at 250 °C with PAN or PPN mixing ratios ≤ 600 pptv. Shorter chain lengths were observed at higher mixing ratios (e.g., 62±2 at 1300 pptv, 53±4 at 2100 pptv, and 48±2 at 2400 pptv, respectively). Thus, the amplification factor is concentration dependent at RO_2 mixing ratios above 600 pptv and is constant under atmospherically relevant trace conditions.

PERCA reactors utilizing CO as a chain carrier show non-linearity at RO_2 mixing ratios above ~200 pptv (Hastie et al., 1991), while room temperature ethane based PERCA have a reported linear dynamic range up to ~800 pptv (Wood et al., 2016). The greater dynamic range with ethane arises because of lower chain lengths and radical concentrations in the reactor and hence reduced radical-radical termination reactions (Wood et al., 2016). The linear range of the ethane TD-PERCA reactor of ~600 pptv falls in between these two extremes, as the CL and radical concentrations are greater than ethane PERCA at room temperature but less than those achievable with CO PERCA. The linear range observed is consistent with box model simulations, in particular when wall loss reactions are taken into account (Figure S-6).

3.5.3 Dependence of chain lengths on inlet temperature

Next, we investigated the temperature dependence of the TD-PERCA-CRDS signal when sampling photochemically generated PNA at constant RH and PNA mixing ratio. Figure 11 shows such a temperature scan of ~180 pptv PNA (measured in parallel by CIMS). The non-amplified TD profile observed by TD-CRDS is superimposed for comparison.

A striking feature in Figure 11 is the very large increase in the amplified NO_2 signal observed at temperatures above ~150 °C. This is an artefact that arises from O_3 co-emitted by the photochemical source and is commented on further in section 3.6.1.

It is obvious from Figure 11 that the amplification factor is strongly dependent on temperature: Even though PNA fully dissociates at temperatures > ~90 °C in our inlets (Figure 4), the amplified signal increases by ~60% in the region from 90 °C to 135 °C (Figure 11, insert), corresponding to amplification factors of ~15 and ~22, respectively. This increase is qualitatively consistent (if extrapolated) with the higher amplification factor observed with PAN or PPN at 250 °C.

Box model simulations using only gas-phase chemistry from the MCM V3.3.1 (Figure S-3) show that the CL is expected to decrease with increasing temperature, opposite to what is observed. This occurs in the model because the chain-carrying reactions of HO_2 and RO_2 with NO (e.g., R3, Table 3) have negative activation energies and are hence slower at higher temperatures, yielding a lower CL at higher temperature. This is partially offset when the chemistry of $HO_2 \cdot H_2O$ is added to the mechanism (Figures S-4 and S-5) but does not suffice to achieve a higher CL at higher temperature; the latter is only predicted by the box model simulations if much lower wall loss reactivity of OH and HO_2 are assumed (see S1.3 and S1.4).

3.6 Interferences

3.6.1 Interference from O_3 in the measurement of ΣPAN at 250 °C

When sampling ambient air (data not shown) or when sampling photochemically generated PNA (Figure 11) the amplified NO_2 increases sharply at PERCA inlet temperatures above ~150 °C. These observations can be rationalized by thermal decomposition of O_3. Even though only a small fraction of O_3 dissociates to O_2 + O at ~150 °C in the TD inlet (~0.1%; Figure 5 (Jones and Davidson, 1962; Heimerl and Coffee, 1979)), a comparatively large signal is generated because the O atom reacts with C_2H_6 to form two radicals, OH and C_2H_5 (Baulch et al., 1994). This reaction is competitive in the PERCA inlet (compared to reaction of O with O_2) because of the high C_2H_6 concentration (1.7%): The lifetime of O with respect to reaction with C_2H_6 is ~0.34 ms, which is of similar magnitude as the expected lifetime of O with respect to reaction with O_2 of ~0.15 ms (Hippler et al., 1990).

We considered an alternate inlet configuration in which the inlet length between the NO and ethane addition points is increased to allow for sufficient residence time completely titrate O_3 with the added NO. However, at the optimum NO mixing ratio for PERCA, the 1/e lifetime of O_3 is ~6 s, making this approach unfeasible.

Hence, if O_3 is sampled with an ethane-based TD-PERCA instrument heated above 150 °C, radicals are generated that are amplified by PERCA. Since O_3 is typically present at mixing ratios in the tens of ppbv in ambient air, quantification of ΣPAN with an ethane-based TD-PERCA-CRDS would be challenging. In contrast, TD-PERCA instruments using CO will not have this limitation, as CO reacts with O to CO_2 and would not generate RO_x radicals.

3.6.2 Interference from peroxyacetic acid in the measurement of ΣPAN at 250 °C

In a previous paper (Taha et al., 2018), we reported interference from peroxyacetic acid (PAA) when the inlet was operated at 250 °C. However, the mixing ratios delivered on those experiments were well above what is expected in ambient air. Further, it is unclear what fraction of PAA dissociates at 250 °C, since the Arrhenius parameters for TD of PAA are uncertain (Table 4). Regardless of whose Arrhenius parameters are assumed, the temperature needed to dissociate 0.1% of PAA is greater than that needed to dissociate 99.9% of PAN (Table 4). In ambient air, PAA is present at concentrations of up to one order of magnitude greater than that of PAN (Phillips et al., 2013). We estimate that under typical conditions, the interference from PAA dissociation is <1% and likely be completed prevented if the inlet is operated at a temperature below 250 °C.

3.6.3 Interference from ΣPAN in the measurement of ΣPN at 95 °C – 110 °C

A temperature of 95°C (110 °C) is required to dissociate >90% (>99.9%) of PNA in the TD-PERCA inlet; at these temperatures, ~12% (~39%) of PAN dissociates (Figure 4). Since [PAN] > [PNA] (Table 1) and hence ΣPAN > ΣPN in most environments, the contribution of ΣPAN to the ΣPN signal in ambient air is substantial (and likely also variable given the slope of the PAN TD curve in this region). Hence, measurement of ΣPN in ambient air by TD-PERCA-CRDS with a single channel relative to an NO_2 background measurement is unfeasible.

3.7 Differential temperature TD-PERCA-CRDS for measurement of ΣPN and ΣPAN

3.7.1 Synthetic air mixtures

To overcome the limitations outlined in section 3.6, a multichannel, differential temperature approach was used. Here, two channels were operated at constant temperatures set in the 60 °C to 110 °C range to avoid the interference from O_3 dissociation and ensure that response for ΣPAN remains linear (by dissociating only a fraction of its concentration). Since the amount of NO_2 generated by TD-PERCA is a function of temperature and radical chain length (CL_T) as well as a fraction dissociated (F_T) of PNA and ΣPAN, the responses in the two PERCA channels operated at different temperatures, T1 and T2, are:

$$[NO_2]_{T1} = CL_{T1}\times F_{PAN,T1}\times[\Sigma PAN] + CL_{T1}\times F_{PNA,T1}\times[\Sigma PN] + [NO_2]_{ref} \quad (1a)$$

$$[NO_2]_{T2} = CL_{T2}\times F_{PAN,T2}\times[\Sigma PAN] + CL_{T2}\times F_{PNA,T2}\times[\Sigma PN] + [NO_2]_{ref} \quad (1b)$$

If the CL_T and F_T values are measured at temperatures T1 and T2 independently (i.e., offline), and $[NO_2]_{ref}$ is quantified in an unheated, parallel reference channel, the mixing ratios of ΣPN and ΣPAN can be calculated by rearranging equations (1a) and (1b):

$$[\Sigma PAN] = \frac{([NO_2]_{T1}\text{-}[NO_2]_{ref})\times CL_{T2}F_{PNA,T2}\text{-}([NO_2]_{T2}\text{-}[NO_2]_{ref})\times CL_{T1}F_{PNA,T1}}{CL_{T2}F_{PNA,T2}\times CL_{T1}F_{PAN,T1}\text{-}CL_{T2}F_{PAN,T2}\times CL_{T1}F_{PNA,T1}} \quad (2a)$$

$$[\ \Sigma PN] = \frac{([NO_2]_{T2}\text{-}[NO_2]_{ref})\text{-}CL_{T2}F_{PAN,T2}\times[\Sigma PAN]}{CL_{T2}F_{PNA,T2}} \quad (2b)$$

A time series demonstrating this approach using the four channel setup is presented in Figure 12A. Here, a constant mixing ratio of PNA (along with NO_2 and O_3 from the photolysis source) was added to the inlet between 21:44 and 21:55. At 21:48:30 and at 21:50:45, PAN was added via the GC pre-column. The product of CL and F for PAN and PNA at 110 °C, 80 °C, and 60 °C was determined offline and are summarized in Table 5 and assumed for same for all ΣPN and ΣPAN species.

The time series of PNA and PAN mixing ratios derived from equations 2a and 2b are presented in Figure 12B. Consistent results were obtained independent of which pair of channels was used in the calculations (Table 6).

3.7.2 Laboratory air

The differential temperature TD-PERCA-CRDS was then used to sample and determine ΣPN and ΣPAN in laboratory air. The calibration parameters summarized in Table 5 were used since they were determined with scrubbed air, which has the same RH as the air intake (i.e., the laboratory). The results are summarized in Table 7. The calculated room air ΣPN values mixing ratios are negative (i.e., not physically possible). On the other hand, the ΣPAN mixing ratios are unreasonably large as we have never observed similarly high mixing ratios in our laboratory by GC, TD-CRDS, or by CIMS. Taken together, these observations suggest that there is (or are) species that dissociate in the TD inlet and generate RO_x radicals or, perhaps, atomic oxygen other than ΣPAN. These unknown interfering species seem to have different TD profiles than PAN and PNA as the differential response differs when different pairs of channels are used in the calculation. Furthermore, the response to the unknown species is more prominent when the hottest (110 °C) channel is used in the calculation.

When ~260 pptv of PNA and ~480 pptv PAN (using the same setup as for Figure 12 and Table 6) were added to the sampled laboratory air, the responses (i.e., Δ(ΣPN) and Δ(ΣPAN) are consistent in all channels, which suggests that the chain lengths and dissociated fractions had not changed. This observation corroborates that the ethane based TD-PERCA-CRDS in reality quantifies ΣPAN*, which includes PAN, PPN, etc. plus one or more unidentified species. In section 4, we speculate as to the potential identity of the interfering species.

3.8 Figures of merit

The ability of TD-PERCA-CRDS to detect radicals is limited by the instrument's ability to detect differences in NO_2 concentration after amplification, calculated using (Brown et al., 2002):

$$[\mathrm{NO_2}]_{\mathrm{min}} = \frac{\mathrm{R_L}}{c\sigma_{\mathrm{NO2}}}\left(\frac{\Delta\tau_{\mathrm{min}}}{\tau_0^2}\right) \qquad (3)$$

Here, $[NO_2]_{min}$ is the smallest NO_2 concentration that can be detected, $\Delta\tau_{min}$ is the smallest measurable difference between ring-down time constants in the presence (τ) and absence (τ_0) of NO_2, c is the speed of light, σ_{NO2} is the NO_2 absorption cross-section at 405 nm (6.1×10^{19} cm^2 $molecule^{-1}$ (Paul and Osthoff, 2010)), and R_L is a correction factor. At the 1σ level, $\Delta\tau_{min}$ is approximately (Brown et al., 2002):

$$\Delta\tau_{\mathrm{min}} = \sqrt{2}\times\sigma(\tau_0) \qquad (4)$$

The precision of the NO_2 measurement (and hence the LOD) varied slightly between detection channels and from day to day. Typically, when sampling zero air, the LOD for NO_2 was ~100 pptv (1 s, 2 σ). In the presence of NO and ethane reagent gases, the LOD was larger, typically ~174 pptv (1 s, 2 σ).

Employing the dual-channel-TD-PERCA-CRDS with the PERCA heater at 250 °C, a CL of 69 factored in, and in the absence of NO_2, the (1 s, 2 σ) LOD for ΣPAN* (calculated on the basis of observed precision after subtraction of the reference channel signal, multiplying by $2\sqrt{2}$, and dividing this precision by the CL) was 2.6 pptv. At an inlet temperature of 120 °C and with a CL of 26, the LOD for PNA was 6.8 pptv. When averaging for 90 s, the minimum of an Allan variance plot (Figure 7 of Paul and Osthoff (2010)) the LOD improved to 17 pptv for NO_2, 0.26 pptv for ΣPAN*, and 0.66 pptv for PNA. Under field conditions, where NO, NO_2 and O_3 concentration vary, the LOD is expected to be higher, though this was not evaluated in this work.

The accuracy of TD-PERCA-CRDS is limited by uncertainties in CL (±7% for dry air), variability in the response to different type of peroxy radicals (±9%) (Wood et al., 2016), and of the NO_2 measurement (±4%) which is dominated by uncertainties in the absorption cross-section and R_L (Paul and Osthoff, 2010). Adding these in quadrature gives a combined uncertainty of ±12% for dry air.

An additional uncertainty factor for the differential temperature TD-PERCA-CRDS is the uncertainty in F_T. The chambers are operated at temperatures where F_T is highly sensitive to temperature (Figure 4). Judging from the scatter observed (for example, in Table 6), we estimate that an additional ±5% random error is introduced, raising the combined measurement uncertainty to ±13%. Not included in this estimate are systematic errors that might arise from the unknown and potentially variable TD profile of the interferences included in ΣPAN*.

4 Discussion

The main goal of this work was to evaluate the feasibility of using ethane-based TD-PERCA to quantify ΣPN and ΣPAN in ambient air. This work has identified several stumbling blocks that on aggregate insinuate that such a measurement would be difficult and error-prone in practice.

On the one hand, the ethane-based TD-PERCA-CRDS has demonstrated great LODs (<1 pptv for ΣPAN* and PNA). This constitutes a considerable improvement compared to our previous generation TD-CRDS, whose LOD was in the hundreds of pptv (Paul and Osthoff, 2010), and represents the first optical absorption measurement of PNA at concentration levels of the same magnitude as found in ambient air (Table 1). In addition, the measurement can tolerate a large NO_2 background through selective amplification of the desired signal: In Figure 12, for example, the NO_2 background was >30 ppbv, yet PNA and PAN were quantified with a 1 s, 1 σ precision of <6 pptv and <40 pptv, respectively (Table 6). Moreover, the sensitivity of the ethane-based TD-PERCA is better than the room temperature measurement of RO_x radicals (1.6 pptv; 90 s, 2 σ) (Wood et al., 2016), mainly because of the greater amplification (~69 vs. ~25) and in spite of the CAPS sensor being slightly more sensitive to NO_2 than our CRDS. Furthermore, the instrument's sensitivity is comparable to (or better than) what is achievable with commonly used GC and CIMS methods. For example, at an inline temperature of 120 °C, the sensitivity of TD-PERCA-CRDS for PNA was of the same order of magnitude as our CIMS at its non-specific ion at *m/z* 62 and the optimized CIMS recently described by Chen et al. (2017a).

The TD-PERCA-CRDS owes its good sensitivity to its high CL, which increases with temperature. Our attempts to rationalize the temperature through model simulations (see S.I.) were limited because models simulating PERCA need to take wall loss rates into account and are generally poor predictors of experimental chain lengths. From a gas-phase kinetics perspective, reactions of HO_2 and RO_2 with NO (e.g., R3, Table 3) have a negative activation energy and are thus expected to slow down at higher temperatures, decreasing turnover rates and the CL. On the over hand, the RH dependence is reduced by heating, in part because one of the radical chain-terminating reaction, $HO_2+NO \rightarrow HNO_3$, proceeds via a water adduct ($HO_2 \cdot H_2O$) (Butkovskaya et al., 2007; Butkovskaya et al., 2009). The temperatures within the PERCA reaction heater are sufficiently elevated to dissociate this intermediate, shutting down this radical sink reaction. In addition, the elevated temperatures inside the reactor may lessen reactions at the reactor inner wall surfaces (by driving off adsorbed water molecules, for example) though we lack direct evidence for this happening.

On the other hand, however, the TD-PERCA-CRDS method has several drawbacks, some of which still need to be overcome to make ambient measurements a reality.

The first challenge is posed by the TD profiles of PAN and PNA (Figure 4) which are not completely separated. This overlap is particularly problematic in ambient air because the signal generated by the typically much smaller PNA concentrations could be overshadowed by a much larger ΣPAN signal. In this work, the overlap of the TD profiles of PNA and PAN (and, the rather limited dynamic range of <500 pptv) was overcome by the differential temperature / linear combination method (section 3.7) in which ΣPAN was only partially dissociated and PNA close to completely dissociated.

A complication is that methyl and ethyl peroxy nitrate have TD profiles that are similar, but not identical, to that of PNA; these molecules dissociate at lower temperatures than PNA (Table 4). This does not matter if the TD-PERCA inlets are operated at temperatures at which all three molecules are fully dissociated (or nearly so) as in this work.

The differential temperature approach has the additional advantage of avoiding the O_3 interference that occurs above 150 °C, which would otherwise have been a serious issue because of the typically much larger O_3 than PAN or PNA concentrations in ambient air, and gave consistent results in synthesized air mixtures and room air.

A second drawback of TD-PERCA is the RH dependent CL, which necessitates frequent calibrations to determine CL×F at each channel's temperature, though this could in principle be straightforward with photochemical sources of PNA and PAN and automated switching. At the same time, frequent calibrations of CL and F would relax the need to carefully match the responses in each of the TD channels, which is a requirement in conventional TD instruments.

A third and most substantial drawback are the interferences. The O_3 interference is easily avoided by switching the instrument from ethane to CO operation. With CO, any O generated from O_3 dissociation would react to form CO_2 and be of no further consequence. However, CO-PERCA is somewhat unappealing because of CO's high toxicity and lack of smell, making its use impractical and impermissible in some university laboratories due to legitimate safety concerns. Mihele and Hastie (2000) used PAN as a radical source by heating a short section of the inlet of their CO-PERCA to 200 °C and found the CL to be the same as other radical sources (which included passing H_2 past a heated wire and a Cl_2 photolysis source), which suggests that the CL in a CO based PERCA is less dependent on temperature than with an ethane based PERCA, which would be another advantage of CO based PERCA.

The unknown interference observed in laboratory air is by far the biggest hurdle. We do not know the identity of the molecule or class of molecules interfering, and if the interference is present in ambient air, away from anthropogenic sources, or found only within a chemistry laboratory. We previously reported (Taha et al., 2018) that the ethane-based TD-PERCA-CRDS responds to peroxide explosives and also responds when sampling the head space above common skin cream and moisturizer products, which contain organosiloxanes. Organosiloxanes have become ubiquitous in the environment and have been found in indoor air in ppbv levels (Rücker and Kümmerer, 2015). Their barriers to dissociation have been reported (Davidson and Thompson, 1971) and are too large for decomposition to occur at the inlet temperatures used in this work. However, Kulyk et al. (2016) recently suggested that pyrolysis of certain polysiloxanes may occur at temperatures as low as 70 °C. Clearly, more work is needed to identify which molecules or class of molecules interferes in TD-PERCA-CRDS and are included in ΣPAN*. It is possible that the interfering species thermally dissociate(s) to release O atoms; if that's the case, this interference would not be present in a CO based TD-PERCA. Hence, measurements using a CO-based TD-PERCA should be attempted. Furthermore, such measurements should be complemented by parallel measurements of PNA, PAN and PPN by CIMS.

Acknowledgments

This work was made possible by the financial support of the National Science and Engineering Research Council of Canada (NSERC) in the form of a Discovery grant. The authors thank Ezra Wood for sharing a preprint version of a manuscript and useful discussions. YMT, CZY, and NMG acknowledge financial support from the NSERC Collaborative Research and Training Experience Program (CREATE) "Integrating Atmospheric Chemistry and Physics from Earth to Space" (IACPES) and QEII graduate scholarships.

References

Abida, O., Mielke, L. H., and Osthoff, H. D.: Observation of gas-phase peroxynitrous and peroxynitric acid during the photolysis of nitrate in acidified frozen solutions, Chem. Phys. Lett., 511, 187-192, 10.1016/j.cplett.2011.06.055 2011.

Ahmadov, R., McKeen, S., Trainer, M., Banta, R., Brewer, A., Brown, S., Edwards, P. M., de Gouw, J. A., Frost, G. J., Gilman, J., Helmig, D., Johnson, B., Karion, A., Koss, A., Langford, A., Lerner, B., Olson, J., Oltmans, S., Peischl, J., Pétron, G., Pichugina, Y., Roberts, J. M., Ryerson, T., Schnell, R., Senff, C., Sweeney, C., Thompson, C., Veres, P. R., Warneke, C., Wild, R., Williams, E. J., Yuan, B., and Zamora, R.: Understanding high wintertime ozone pollution events in an oil- and natural gas-producing region of the western US, Atmos. Chem. Phys., 15, 411-429, 10.5194/acp-15-411-2015, 2015.

Atkinson, R., Baulch, D. L., Cox, R. A., Hampson, R. F., Kerr, J. A., Rossi, M. J., and Troe, J.: Evaluated kinetic, photochemical and heterogeneous data for atmospheric chemistry .5. IUPAC Subcommittee on Gas Kinetic Data Evaluation for Atmospheric Chemistry, Journal Of Physical And Chemical Reference Data, 26, 521-1011, 10.1063/1.556011, 1997.

Bates, D. R., and Nicolet, M.: The photochemistry of atmospheric water vapor, J. Geophys. Res., 55, 301-327, 10.1029/JZ055i003p00301, 1950.

Baulch, D. L., Cobos, C. J., Cox, R. A., Frank, P., Hayman, G., Just, T., Kerr, J. A., Murrells, T., Pilling, M. J., Troe, J., Walker, R. W., and Warnatz, J.: Summary table of evaluated kinetic data for combustion modeling: Supplement 1, Combustion and Flame, 98, 59-79, 10.1016/0010-2180(94)90198-8, 1994.

Blanchard, P., Shepson, P. B., Schiff, H. I., and Drummond, J. W.: Development of a gas-chromatograph for trace-level measurement of peroxyacetyl nitrate using chemical amplification, Anal. Chem., 65, 2472-2477, 10.1021/ac00066a012, 1993.

Brown, S. S., Stark, H., Ciciora, S. J., McLaughlin, R. J., and Ravishankara, A. R.: Simultaneous in situ detection of atmospheric NO_3 and N_2O_5 via cavity ring-down spectroscopy, Rev. Sci. Instrum., 73, 3291-3301, 10.1063/1.1499214, 2002.

Butkovskaya, N., Kukui, A., and Le Bras, G.: HNO_3 forming channel of the HO_2+NO reaction as a function of pressure and temperature in the ranges of 72-600 Torr and 223-323 K, J. Phys. Chem. A, 111, 9047-9053, 10.1021/jp074117m, 2007.

Butkovskaya, N., Rayez, M. T., Rayez, J. C., Kukui, A., and Le Bras, G.: Water Vapor Effect on the HNO_3 Yield in the HO_2 + NO Reaction: Experimental and Theoretical Evidence, J. Phys. Chem. A, 113, 11327-11342, 10.1021/jp811428p, 2009.

Cantrell, C. A., Stedman, D. H., and Wendel, G. J.: Measurement of atmospheric peroxy-radicals by chemical amplification, Anal. Chem., 56, 1496-1502, 10.1021/ac00272a065, 1984.

Cantrell, C. A., Shetter, R. E., and Calvert, J. G.: Dual-inlet chemical amplifier for atmospheric peroxy radical measurements, Anal. Chem., 68, 4194-4199, 10.1021/ac960639e, 1996.

Chen, D. X., Huey, L. G., Tanner, D. J., Li, J. F., Ng, N. L., and Wang, Y. H.: Derivation of Hydroperoxyl Radical Levels at an Urban Site via Measurement of Pernitric Acid by Iodide Chemical Ionization Mass Spectrometry, Environm. Sci. Technol., 51, 3355-3363, 10.1021/acs.est.6b05169, 2017a.

Chen, G., Davis, D., Crawford, J., Hutterli, L. M., Huey, L. G., Slusher, D., Mauldin, L., Eisele, F., Tanner, D., Dibb, J., Buhr, M., McConnell, J., Lefer, B., Shetter, R., Blake, D., Song, C. H., Lombardi, K., and Arnoldy, J.: A reassessment of HOx South Pole chemistry based on observations recorded during ISCAT 2000, Atmos. Environm., 38, 5451-5461, 10.1016/j.atmosenv.2003.07.018, 2004.

Chen, J., Wu, H., Liu, A. W., Hu, S. M., and Zhang, J.: Field Measurement of NO_2 and RNO_2 by Two-Channel Thermal Dissociation Cavity Ring Down Spectrometer, Chin. J. Chem. Phys., 30, 493-498, 10.1063/1674-0068/30/cjcp1705084, 2017b.

Crounse, J. D., Nielsen, L. B., Jorgensen, S., Kjaergaard, H. G., and Wennberg, P. O.: Autoxidation of Organic Compounds in the Atmosphere, Journal of Physical Chemistry Letters, 4, 3513-3520, 10.1021/jz4019207, 2013.

Davidson, I. M. T., and Thompson, J. F.: Dimethylsilanone from the pyrolysis of octamethylcyclotetrasiloxane, Journal of the Chemical Society D: Chemical Communications, 251-252, 10.1039/c29710000251, 1971.

Davis, D., Chen, G., Buhr, M., Crawford, J., Lenschow, D., Lefer, B., Shetter, R., Eisele, F., Mauldin, L., and Hogan, A.: South Pole NO_x chemistry: an assessment of factors controlling variability and absolute levels, Atmos. Environm., 38, 5375-5388, 10.1016/j.atmosenv.2004.04.039, 2004.

Day, D. A., Wooldridge, P. J., Dillon, M. B., Thornton, J. A., and Cohen, R. C.: A thermal dissociation laser-induced fluorescence instrument for in situ detection of NO_2, peroxy nitrates, alkyl nitrates, and HNO_3, J. Geophys. Res., 107, D6, 4046, 10.1029/2001JD000779, 2002.

Devush, S. S., Prisyazhnyuk, Z. P., and Kovalskaya, A. M.: Kinetics of the thermal gas-phase decomposition of C1-C4 organic peracids, Kinet. Catal., 24, 1098-1101, 1983.

Di Carlo, P., Aruffo, E., Busilacchio, M., Giammaria, F., Dari-Salisburgo, C., Biancofiore, F., Visconti, G., Lee, J., Moller, S., Reeves, C. E., Bauguitte, S., Forster, G., Jones, R. L., and Ouyang, B.: Aircraft based four-channel thermal dissociation laser induced fluorescence instrument for simultaneous measurements of NO_2, total peroxy nitrate, total alkyl nitrate, and HNO_3, Atmospheric Measurement Techniques, 6, 971-980, 10.5194/amt-6-971-2013, 2013.

Dusanter, S., Vimal, D., Stevens, P. S., Volkamer, R., and Molina, L. T.: Measurements of OH and HO2 concentrations during the MCMA-2006 field campaign – Part 1: Deployment of the Indiana University laser-induced fluorescence instrument, Atmos. Chem. Phys., 9, 1665-1685, 10.5194/acp-9-1665-2009, 2009.

Edwards, G. D., Cantrell, C. A., Stephens, S., Hill, B., Goyea, O., Shetter, R. E., Mauldin, R. L., Kosciuch, E., Tanner, D. J., and Eisele, F. L.: Chemical ionization mass spectrometer instrument for the measurement of tropospheric HO_2 and RO_2, Anal. Chem., 75, 5317-5327, 10.1021/ac034402b, 2003.

Ehn, M., Thornton, J. A., Kleist, E., Sipila, M., Junninen, H., Pullinen, I., Springer, M., Rubach, F., Tillmann, R., Lee, B., Lopez-Hilfiker, F., Andres, S., Acir, I.-H., Rissanen, M., Jokinen, T., Schobesberger, S., Kangasluoma, J., Kontkanen, J., Nieminen, T., Kurten, T., Nielsen, L. B., Jorgensen, S., Kjaergaard, H. G., Canagaratna, M., Maso, M. D., Berndt, T., Petaja, T., Wahner, A., Kerminen, V.-M., Kulmala, M., Worsnop, D. R., Wildt, J., and Mentel, T. F.: A large source of low-volatility secondary organic aerosol, Nature, 506, 476-479, 10.1038/nature13032, 2014.

Eisele, F., Davis, D. D., Helmig, D., Oltmans, S. J., Neff, W., Huey, G., Tanner, D., Chen, G., Crawford, J., Arimoto, R., Buhr, M., Mauldin, L., Hutterli, M., Dibb, J., Blake, D., Brooks, S. B., Johnson, B., Roberts, J. M., Wang, Y. H., Tan, D., and Flocke, F.: Antarctic Tropospheric Chemistry Investigation (ANTCI) 2003 overview, Atmospheric Environment, 42, 2749-2761, 10.1016/j.atmosenv.2007.04.013, 2008.

Faloona, I. C., Tan, D., Lesher, R. L., Hazen, N. L., Frame, C. L., Simpas, J. B., Harder, H., Martinez, M., Di Carlo, P., Ren, X. R., and Brune, W. H.: A laser-induced fluorescence instrument for detecting tropospheric OH and HO_2: Characteristics and calibration, J. Atmos. Chem., 47, 139-167, 10.1023/B:JOCH.0000021036.53185.0e, 2004.

Fleming, Z. L., Monks, P. S., Rickard, A. R., Heard, D. E., Bloss, W. J., Seakins, P. W., Still, T. J., Sommariva, R., Pilling, M. J., Morgan, R., Green, T. J., Brough, N., Mills, G. P., Penkett, S. A., Lewis, A. C., Lee, J. D., Saiz-Lopez, A., and Plane, J. M. C.: Peroxy radical chemistry and the control of ozone photochemistry at Mace Head, Ireland during the summer of 2002, Atmos. Chem. Phys., 6, 2193-2214, 10.5194/acp-6-2193-2006, 2006.

Fuchs, H., Holland, F., and Hofzumahaus, A.: Measurement of tropospheric RO_2 and HO_2 radicals by a laser-induced fluorescence instrument, Rev. Sci. Instrum., 79, 084104-084112, 10.1063/1.2968712, 2008.

Fuchs, H., Dubé, W. P., Lerner, B. M., Wagner, N. L., Williams, E. J., and Brown, S. S.: A Sensitive and Versatile Detector for Atmospheric NO_2 and NO_x Based on Blue Diode Laser Cavity Ring-Down Spectroscopy, Environm. Sci. Technol., 43, 7831-7836, 10.1021/es902067h, 2009.

Furgeson, A., Mielke, L. H., Paul, D., and Osthoff, H. D.: A photochemical source of peroxypropionic and peroxyisobutanoic nitric anhydride, Atmos. Environm., 45, 5025-5032, 10.1016/j.atmosenv.2011.03.072, 2011.

Green, T. J., Reeves, C. E., Fleming, Z. L., Brough, N., Rickard, A. R., Bandy, B. J., Monks, P. S., and Penkett, S. A.: An improved dual channel PERCA instrument for atmospheric measurements of peroxy radicals, J. Environ. Monit., 8, 530-536, 10.1039/B514630E 2006.

Grosjean, D., Grosjean, E., and Williams, E. L.: Thermal decomposition of PAN, PPN and vinyl-PAN, J. Air Waste Manag. Assoc., 44, 391-396, 10.1080/1073161X.1994.10467260, 1994.

Hanke, M., Uecker, J., Reiner, T., and Arnold, F.: Atmospheric peroxy radicals: ROXMAS, a new mass-spectrometric methodology for speciated measurements of HO_2 and Sigma RO_2 and first results, Int. J. Mass Spectrom., 213, 91-99, 10.1016/s1387-3806(01)00548-6, 2002.

Hastie, D. R., Weissenmayer, M., Burrows, J. P., and Harris, G. W.: Calibrated chemical amplifier for atmospheric RO_x measurements, Anal. Chem., 63, 2048-2057, 10.1021/ac00018a029, 1991.

Heard, D. E.: Atmospheric field measurements of the hydroxyl radical using laser-induced fluorescence spectroscopy, Ann. Rev. Phys. Chem., 57, 191-216, 10.1146/annurev.physchem.57.032905.104516, 2006.

Heimerl, J. M., and Coffee, T. P.: The unimolecular ozone decomposition reaction, Combustion and Flame, 35, 117-123, 10.1016/0010-2180(79)90015-4, 1979.

Hippler, H., Rahn, R., and Troe, J.: Temperature and pressure dependence of ozone formation rates in the range 1–1000 bar and 90–370 K, The Journal of Chemical Physics, 93, 6560-6569, 10.1063/1.458972, 1990.

Hornbrook, R. S., Crawford, J. H., Edwards, G. D., Goyea, O., Mauldin Iii, R. L., Olson, J. S., and Cantrell, C. A.: Measurements of tropospheric HO_2 and RO_2 by oxygen dilution modulation and chemical ionization mass spectrometry, Atmos. Meas. Tech., 4, 735-756, 10.5194/amt-4-735-2011, 2011.

Horstjann, M., Andres Hernandez, M. D., Nenakhov, V., Chrobry, A., and Burrows, J. P.: Peroxy radical detection for airborne atmospheric measurements using absorption spectroscopy of NO_2, Atmos. Meas. Tech., 7, 1245-1257, 10.5194/amt-7-1245-2014, 2014.

Jenkin, M. E., Saunders, S. M., and Pilling, M. J.: The tropospheric degradation of volatile organic compounds: a protocol for mechanism development, Atmos. Environm., 31, 81-104, 10.1016/S1352-2310(96)00105-7, 1997.

Jenkin, M. E., Wyche, K. P., Evans, C. J., Carr, T., Monks, P. S., Alfarra, M. R., Barley, M. H., McFiggans, G. B., Young, J. C., and Rickard, A. R.: Development and chamber evaluation of the MCM v3.2 degradation scheme for β-caryophyllene, Atmos. Chem. Phys., 12, 5275-5308, 10.5194/acp-12-5275-2012, 2012.

Jones, A. E., Brough, N., Anderson, P. S., and Wolff, E. W.: HO_2NO_2 and HNO_3 in the coastal Antarctic winter night: a "lab-in-the-field" experiment, Atmos. Chem. Phys., 14, 11843-11851, 10.5194/acp-14-11843-2014, 2014.

Jones, W. M., and Davidson, N.: The Thermal Decomposition of Ozone in a Shock Tube, J. Am. Chem. Soc., 84, 2868-2878, 10.1021/ja00874a005, 1962.

Kabir, M., Jagiella, S., and Zabel, F.: Thermal Stability of n-Acyl Peroxynitrates, Internat. J. Chem. Kin., 46, 462-469, 10.1002/kin.20862, 2014.

Kanno, N., Tonokura, K., and Koshi, M.: Equilibrium constant of the HO_2-H_2O complex formation and kinetics of HO_2+HO_2-H_2O: Implications for tropospheric chemistry, J. Geophys. Res.-Atmos., 111, D20312, 10.1029/2005jd006805, 2006.

Kim, S., Huey, L. G., Stickel, R. E., Tanner, D. J., Crawford, J. H., Olson, J. R., Chen, G., Brune, W. H., Ren, X., Lesher, R., Wooldridge, P. J., Bertram, T. H., Perring, A., Cohen, R. C., Lefer, B. L., Shetter, R. E., Avery, M., Diskin, G., and Sokolik, I.: Measurement of HO_2NO_2 in the free troposphere during the Intercontinental Chemical Transport Experiment–North America 2004, J. Geophys. Res.-Atmos., 112, D12S01, 10.1029/2006jd007676, 2007.

Kirchner, F., and Stockwell, W. R.: Effect of peroxy radical reactions on the predicted concentrations of ozone, nitrogenous compounds, and radicals, J. Geophys. Res.-Atmos., 101, 21007-21022, 10.1029/96jd01519, 1996.

Kulyk, K., Zettergren, H., Gatchell, M., Alexander, J. D., Borysenko, M., Palianytsia, B., Larsson, M., and Kulik, T.: Dimethylsilanone Generation from Pyrolysis of Polysiloxanes Filled with Nanosized Silica and Ceria/Silica, ChemPlusChem, 81, 1003-1013, 10.1002/cplu.201600229, 2016.

Lee, J. B., Yoon, J. S., Jung, K., Eom, S. W., Chae, Y. Z., Cho, S. J., Kim, S. D., Sohn, J. R., and Kim, K. H.: Peroxyacetyl nitrate (PAN) in the urban atmosphere, Chemosphere, 93, 1796-1803, 10.1016/j.chemosphere.2013.06.019, 2013.

Lee, L., Wooldridge, P. J., deGouw, J., Brown, S. S., Bates, T. S., Quinn, P. K., and Cohen, R. C.: Particulate organic nitrates observed in an oil and natural gas production region during wintertime, Atmos. Chem. Phys., 15, 9313-9325, 10.5194/acp-15-9313-2015, 2015.

Liu, Y., and Zhang, J.: Atmospheric Peroxy Radical Measurements Using Dual-Channel Chemical Amplification Cavity Ringdown Spectroscopy, Anal. Chem., 86, 5391-5398, 10.1021/ac5004689, 2014.

Mielke, L. H., Furgeson, A., and Osthoff, H. D.: Observation of $ClNO_2$ in a mid-continental urban environment, Environm. Sci. Technol., 45, 8889-8896, 10.1021/es201955u, 2011.

Mielke, L. H., and Osthoff, H. D.: On quantitative measurements of peroxycarboxylic nitric anhydride mixing ratios by thermal dissociation chemical ionization mass spectrometry, Int. J. Mass Spectrom., 310, 1-9, 10.1016/j.ijms.2011.10.005, 2012.

Mihele, C. M., and Hastie, D. R.: The sensitivity of the radical amplifier to ambient water vapour, Geophys. Res. Lett., 25, 1911-1913, 10.1029/98gl01432, 1998.

Mihele, C. M., Mozurkewich, M., and Hastie, D. R.: Radical loss in a chain reaction of CO and NO in the presence of water: Implications for the radical amplifier and atmospheric chemistry, Internat. J. Chem. Kin., 31, 145-152, 10.1002/(sici)1097-4601(1999)31:2<145::aid-kin7>3.0.co;2-m, 1999.

Mihele, C. M., and Hastie, D. R.: Optimized operation and calibration procedures for radical amplifier-type detectors, Journal Of Atmospheric And Oceanic Technology, 17, 788-794, 10.1175/1520-0426(2000)017<0788:OOACPF>2.0.CO;2, 2000.

Mills, G. P., Sturges, W. T., Salmon, R. A., Bauguitte, S. J. B., Read, K. A., and Bandy, B. J.: Seasonal variation of peroxyacetylnitrate (PAN) in coastal Antarctica measured with a new instrument for the detection of sub-part per trillion mixing ratios of PAN, Atmos. Chem. Phys., 7, 4589-4599, 10.5194/acp-7-4589-2007, 2007.

Murphy, J. G., Thornton, J. A., Wooldridge, P. J., Day, D. A., Rosen, R. S., Cantrell, C., Shetter, R. E., Lefer, B., and Cohen, R. C.: Measurements of the sum of HO_2NO_2 and $CH_3O_2NO_2$ in the remote troposphere, Atmos. Chem. Phys., 4, 377-384, 10.5194/acp-4-377-2004, 2004.

Odame-Ankrah, C. A., and Osthoff, H. D.: A compact diode laser cavity ring-down spectrometer for atmospheric measurements of NO_3 and N_2O_5 with automated zeroing and calibration, Appl. Spectrosc., 65, 1260-1268, 10.1366/11-06384, 2011.

Odame-Ankrah, C. A.: Improved detection instrument for nitrogen oxide species, Ph.D., Chemistry, University of Calgary, http://hdl.handle.net/11023/2006, 10.5072/PRISM/26475, Calgary, 2015.

Paul, D., Furgeson, A., and Osthoff, H. D.: Measurements of total peroxy and alkyl nitrate abundances in laboratory-generated gas samples by thermal dissociation cavity ring-down spectroscopy, Rev. Sci. Instrum., 80, 114101, 10.1063/1.3258204 2009.

Paul, D., and Osthoff, H. D.: Absolute Measurements of Total Peroxy Nitrate Mixing Ratios by Thermal Dissociation Blue Diode Laser Cavity Ring-Down Spectroscopy, Anal. Chem., 82, 6695-6703, 10.1021/ac101441z, 2010.

Perez, I. M., Wooldridge, P. J., and Cohen, R. C.: Laboratory evaluation of a novel thermal dissociation chemiluminescence method for in situ detection of nitrous acid, Atmos. Environm., 41, 3993-4001, 10.1016/j.atmosenv.2007.01.060, 2007.

Phillips, G. J., Pouvesle, N., Thieser, J., Schuster, G., Axinte, R., Fischer, H., Williams, J., Lelieveld, J., and Crowley, J. N.: Peroxyacetyl nitrate (PAN) and peroxyacetic acid (PAA) measurements by iodide chemical ionisation mass spectrometry: first analysis of results in the boreal forest and implications for the measurement of PAN fluxes, Atmos. Chem. Phys., 13, 1129-1139, 10.5194/acp-13-1129-2013, 2013.

Portmann, R. W., Brown, S. S., Gierczak, T., Talukdar, R. K., Burkholder, J. B., and Ravishankara, A. R.: Role of nitrogen oxides in the stratosphere: A reevaluation based on laboratory studies, Geophys. Res. Lett., 26, 2387-2390, 10.1029/1999GL900499, 1999.

Roberts, J. M.: The atmospheric chemistry of organic nitrates, Atmos. Environm. A, 24, 243-287, 10.1016/0960-1686(90)90108-Y, 1990.

Roberts, J. M.: PAN and Related Compounds, in: Volatile Organic Compounds in the Atmosphere, edited by: Koppmann, R., Blackwell Publishing, Oxford, UK, 221-268, 2007.

Rollins, A. W., Smith, J. D., Wilson, K. R., and Cohen, R. C.: Real Time In Situ Detection of Organic Nitrates in Atmospheric Aerosols, Environm. Sci. Technol., 44, 5540-5545, 10.1021/es100926x, 2010.

Rücker, C., and Kümmerer, K.: Environmental Chemistry of Organosiloxanes, Chem. Rev., 115, 466-524, 10.1021/cr500319v, 2015.

Sadanaga, Y., Takaji, R., Ishiyama, A., Nakajima, K., Matsuki, A., and Bandow, H.: Thermal dissociation cavity attenuated phase shift spectroscopy for continuous measurement of total peroxy and organic nitrates in the clean atmosphere, Rev. Sci. Instrum., 87, 074102, 10.1063/1.4958167, 2016.

Sahetchian, K. A., Rigny, R., Tardieu de Maleissye, J., Batt, L., Anwar Khan, M., and Mathews, S.: The pyrolysis of organic hydroperoxides (ROOH), Symposium (International) on Combustion, 24, 637-643, 10.1016/S0082-0784(06)80078-0, 1992.

Sandu, A., and Sander, R.: Technical note: Simulating chemical systems in Fortran90 and Matlab with the Kinetic PreProcessor KPP-2.1, Atmos. Chem. Phys., 6, 187-195, 10.5194/acp-6-187-2006, 2006.

Saunders, S. M., Jenkin, M. E., Derwent, R. G., and Pilling, M. J.: Protocol for the development of the Master Chemical Mechanism, MCM v3 (Part A): tropospheric degradation of non-aromatic volatile organic compounds, Atmos. Chem. Phys., 3, 161-180, 10.5194/acp-3-161-2003, 2003.

Schmidt, C., and Sehon, A. H.: The thermal decomposition of peracetic acid in the vapor phase, Canadian Journal of Chemistry, 41, 1819-1825, 10.1139/v63-261, 1963.

Singh, H. B., Herlth, D., Ohara, D., Zahnle, K., Bradshaw, J. D., Sandholm, S. T., Talbot, R., Crutzen, P. J., and Kanakidou, M.: Relationship of peroxyacetyl nitrate to active and total odd nitrogen at northern high-latitudes - influence of reservoir species on NO_x and O_3, J. Geophys. Res.-Atmos., 97, 16523-16530, 10.1029/91jd00890, 1992.

Singh, H. B., Brune, W. H., Crawford, J. H., Jacob, D. J., and Russell, P. B.: Overview of the summer 2004 Intercontinental Chemical Transport Experiment–North America (INTEX-A), J. Geophys. Res.-Atmos., 111, D24S01, 10.1029/2006jd007905, 2006.

Slusher, D. L., Pitteri, S. J., Haman, B. J., Tanner, D. J., and Huey, L. G.: A chemical ionization technique for measurement of pernitric acid in the upper troposphere and the polar boundary layer, Geophysical Research Letters, 28, 3875-3878, 10.1029/2001gl013443, 2001.

Slusher, D. L., Huey, L. G., Tanner, D. J., Flocke, F. M., and Roberts, J. M.: A thermal dissociation-chemical ionization mass spectrometry (TD-CIMS) technique for the simultaneous measurement of peroxyacyl nitrates and dinitrogen pentoxide, J. Geophys. Res., 109, D19315, 10.1029/2004JD004670, 2004.

Sobanski, N., Schuladen, J., Schuster, G., Lelieveld, J., and Crowley, J. N.: A five-channel cavity ring-down spectrometer for the detection of NO_2, NO_3, N_2O_5, total peroxy nitrates and total alkyl nitrates, Atmos. Meas. Tech., 9, 5103-5118, 10.5194/amt-9-5103-2016, 2016.

Solomon, S.: Stratospheric ozone depletion: A review of concepts and history, Rev. Geophys., 37, 275-316, 10.1029/1999RG900008, 1999.

Spencer, K. M., McCabe, D. C., Crounse, J. D., Olson, J. R., Crawford, J. H., Weinheimer, A. J., Knapp, D. J., Montzka, D. D., Cantrell, C. A., Hornbrook, R. S., Mauldin, R. L., and Wennberg, P. O.: Inferring ozone production in an urban atmosphere using measurements of peroxynitric acid, Atmos. Chem. Phys., 9, 3697-3707, 10.5194/acp-9-3697-2009, 2009.

Stenke, A., and Grewe, V.: Simulation of stratospheric water vapor trends: impact on stratospheric ozone chemistry, Atmos. Chem. Phys., 5, 1257-1272, 10.5194/acp-5-1257-2005, 2005.

Taha, Y. M., Saowapon, M. T., and Osthoff, H. D.: Detection of triacetone triperoxide by thermal decomposition peroxy radical chemical amplification coupled to cavity ring-down spectroscopy, Anal. Bioanal. Chem., 410, 4203-4212, 10.1007/s00216-018-1072-0, 2018.

Thaler, R. D., Mielke, L. H., and Osthoff, H. D.: Quantification of Nitryl Chloride at Part Per Trillion Mixing Ratios by Thermal Dissociation Cavity Ring-Down Spectroscopy, Anal. Chem., 83, 2761-2766, 10.1021/ac200055z, 2011.

Thieser, J., Schuster, G., Schuladen, J., Phillips, G. J., Reiffs, A., Parchatka, U., Pöhler, D., Lelieveld, J., and Crowley, J. N.: A two-channel thermal dissociation cavity ring-down spectrometer for the detection of ambient NO_2, RO_2NO_2 and $RONO_2$, Atmos. Meas. Tech., 9, 553-576, 10.5194/amt-9-553-2016, 2016.

Tokarek, T. W., Huo, J. A., Odame-Ankrah, C. A., Hammoud, D., Taha, Y. M., and Osthoff, H. D.: A gas chromatograph for quantification of peroxycarboxylic nitric anhydrides calibrated by thermal dissociation cavity ring-down spectroscopy, Atmos. Meas. Tech., 7, 3263-3283, 10.5194/amt-7-3263-2014, 2014.

Tuazon, E. C., Winer, A. M., and Pitts, J. N.: Trace pollutant concentrations in a multiday smog episode in the California South Coast Air Basin by long path length Fourier transform infrared spectroscopy, Environm. Sci. Technol., 15, 1232-1237, 10.1021/es00092a014, 1981.

Veres, P. R., Roberts, J. M., Wild, R. J., Edwards, P. M., Brown, S. S., Bates, T. S., Quinn, P. K., Johnson, J. E., Zamora, R. J., and de Gouw, J.: Peroxynitric acid (HO_2NO_2) measurements during the UBWOS 2013 and 2014 studies using iodide ion chemical ionization mass spectrometry, Atmos. Chem. Phys., 15, 8101-8114, 10.5194/acp-15-8101-2015, 2015.

Wild, R. J., Edwards, P. M., Dube, W. P., Baumann, K., Edgerton, E. S., Quinn, P. K., Roberts, J. M., Rollins, A. W., Veres, P. R., Warneke, C., Williams, E. J., Yuan, B., and Brown, S. S.: A Measurement of Total Reactive Nitrogen, NO_y, together with NO_2, NO, and O_3 via Cavity Ring-down Spectroscopy, Environm. Sci. Technol., 48, 9609-9615, 10.1021/es501896w, 2014.

Womack, C. C., Neuman, J. A., Veres, P. R., Eilerman, S. J., Brock, C. A., Decker, Z. C. J., Zarzana, K. J., Dube, W. P., Wild, R. J., Wooldridge, P. J., Cohen, R. C., and Brown, S. S.: Evaluation of the accuracy of thermal dissociation CRDS and LIF techniques for atmospheric measurement of reactive nitrogen species, Atmos. Meas. Tech. Discuss., 2016, 1-30, 10.5194/amt-2016-398, 2016.

Womack, C. C., Neuman, J. A., Veres, P. R., Eilerman, S. J., Brock, C. A., Decker, Z. C. J., Zarzana, K. J., Dube, W. P., Wild, R. J., Wooldridge, P. J., Cohen, R. C., and Brown, S. S.: Evaluation of the accuracy of thermal dissociation CRDS and LIF techniques for atmospheric measurement of reactive nitrogen species, Atmos. Meas. Tech., 10, 1911-1926, 10.5194/amt-10-1911-2017, 2017.

Wood, E. C., Deming, B. L., and Kundu, S.: Ethane-Based Chemical Amplification Measurement Technique for Atmospheric Peroxy Radicals, Environmental Science & Technology Letters, 4, 15-19, 10.1021/acs.estlett.6b00438, 2016.

Wooldridge, P. J., Perring, A. E., Bertram, T. H., Flocke, F. M., Roberts, J. M., Singh, H. B., Huey, L. G., Thornton, J. A., Wolfe, G. M., Murphy, J. G., Fry, J. L., Rollins, A. W., LaFranchi, B. W., and Cohen, R. C.: Total Peroxy Nitrates (ΣPNs) in the atmosphere: the Thermal Dissociation-Laser Induced Fluorescence (TD-LIF) technique and comparisons to speciated PAN measurements, Atmos. Meas. Tech., 3, 593-607, 10.5194/amt-3-593-2010, 2010.

Zheng, W., Flocke, F. M., Tyndall, G. S., Swanson, A., Orlando, J. J., Roberts, J. M., Huey, L. G., and Tanner, D. J.: Characterization of a thermal decomposition chemical ionization mass spectrometer for the measurement of peroxy acyl nitrates (PANs) in the atmosphere, Atmos. Chem. Phys., 11, 6529-6547, 10.5194/acp-11-6529-2011, 2011.

Ziemann, P. J., and Atkinson, R.: Kinetics, products, and mechanisms of secondary organic aerosol formation, Chem. Soc. Rev., 41, 6582-6605, 10.1039/c2cs35122f, 2012.

Tables

Table 1. Typical* PNA and PAN mixing ratios in various environments where both were quantified.

Location	PNA (pptv)	PAN (pptv)	PNA/PAN
Antarctica - Summer	20 (Slusher et al., 2001)	15.6 (Eisele et al., 2008)	1.3
Antarctica - Summer	22 (Jones et al., 2014)	15.6 (Eisele et al., 2008)	1.4
Antarctica – Summer	2.5 (Jones et al., 2014)	9.2 (Mills et al., 2007)	0.27
Remote troposphere – Spring	-	-	0.13** (Murphy et al., 2004)
Free troposphere (Intex-NA) - Summer	45 (Kim et al., 2007)	280 (Singh et al., 2006)	0.16***
Uintah Basin – Winter 2013	500 (Veres et al., 2015)	2000 (Ahmadov et al., 2015)	0.25
Uintah Basin – Winter 2014	100 (Veres et al., 2015)	300 (Lee et al., 2015)	0.33
Atlanta – Winter	3.7 (Chen et al., 2017a)	640-800 (Lee et al., 2013)	<0.01
Atlanta – Summer	11.7 (Chen et al., 2017a)	640-800 (Lee et al., 2013)	0.01-0.02

* Average values

** calculated assuming all non-PAN and PPN peroxy nitrate is PNA.

*** Averages of data posted on ftp://ftp-air.larc.nasa.gov/pub/INTEXA/DC8_AIRCRAFT/

Table 2. Selected thermal dissociation methods for quantification of daytime NO_y species.

Species quantified	NO_2 detection method	Group	Reference
NO_2, ΣPAN, ΣAN, HNO_3	LIF	Berkeley	(Day et al., 2002)
ΣPN	LIF	Berkeley	(Murphy et al., 2004)
HONO	CL	Berkeley	(Perez et al., 2007)
NO_2, ΣPAN, ΣAN	CRDS	Calgary	(Paul et al., 2009)
Aerosol nitrates	LIF	Berkeley	(Rollins et al., 2010)
$ClNO_2$	CRDS	Calgary	(Thaler et al., 2011)
NO_2, ΣPAN, ΣAN, HNO_3	LIF	L'Aquila	(Di Carlo et al., 2013)
NO, NO_2, HONO, NO_y, ammonium nitrate	CRDS	NOAA	(Wild et al., 2014; Womack et al., 2017)
NO_2, ΣPAN, ΣAN	CRDS	Max-Planck-Institut	(Thieser et al., 2016)
NO_2, ΣPAN, ΣAN	CAPS	Osaka	(Sadanaga et al., 2016)
NO_2, RNO_2	CRDS	Hefei	(Chen et al., 2017b)
ΣPN, ΣPAN	PERCA-CRDS	Calgary	this work

Table 3. List of chemical reactions[*]

Number	Reaction	k (cm^3 $molecule^{-1}$ s^{-1})	k_{298K} (cm^3 $molecule^{-1}$ s^{-1})
R1	$CH_3O_2 + NO \rightarrow CH_3O + NO_2$	$2.3\times10^{-12} \times e^{(360/T)}$	7.7×10^{-12}
R2	$CH_3O + O_2 \rightarrow HCHO + HO_2$	$7.2\times10^{-14} \times e^{(-1080/T)}$	1.9×10^{-15}
R3	$HO_2 + NO \rightarrow HO + NO_2$	$3.5\times10^{-12} \times e^{(270/T)}$	8.5×10^{-12}
R4	$C_2H_6 + HO + O_2 \rightarrow H_2O + C_2H_5O_2$	$6.9\times10^{-12} \times e^{(-1000/T)}$	2.4×10^{-13}
R5	$C_2H_5O_2 + NO \rightarrow C_2H_5O + NO_2$	$2.55\times10^{-12} \times e^{(380/T)} \times 0.99$	9.1×10^{-12}
R6	$C_2H_5O + O_2 \rightarrow CH_3CHO + HO_2$	$2.4\times10^{-14} \times e^{(-325/T)}$	8.1×10^{-15}
R7	$PAN \rightarrow CH_3CO_3 + NO_2$	See Table 4	$4.4\times10^{-4}\ s^{-1}$
R8	$CH_3C(O)O_2 + NO \rightarrow NO_2 + CH_3C(O)O \rightarrow NO_2 + CH_3 + CO_2$	$7.5\times10^{-12} \times e^{(290/T)}$	2.0×10^{-11}
R9	$PPN \rightarrow C_2H_5CO_3 + NO_2$	See Table 4	$3.7\times10^{-4}\ s^{-1}$
R10	$C_2H_5CO_3+NO+O_2 \rightarrow C_2H_5O_2+NO_2+CO_2$	$6.7\times10^{-12} \times e^{(340/T)}$	2.1×10^{-11}
R11	$HO + NO + M \rightarrow HONO + M$	$7.4\times10^{-31} \times (T/300)^{-2.4} \times [M]$	9.7×10^{-12} **
R12	$HO_2 + NO_2 + M \rightarrow HO_2NO_2 + M$	(termolecular)	(termolecular)
R13	$HO_2 + HO_2 + M \rightarrow H_2O_2 + M$	(termolecular)	(termolecular)
R14	$CH_3CO_3 \rightarrow 0.7\ CH_3CO_2 + 0.3\ CH_3CO_2H$	$5.0\times10^{-12} \times \sum RO_2$	$5.0\times10^{-12} \times \sum RO_2$
R15	$C_2H_5CO_3 \rightarrow 0.7\ C_2H_5CO_2 + 0.3\ C_2H_5CO_2H$	$5.0\times10^{-12} \times \sum RO_2$	$5.0\times10^{-12} \times \sum RO_2$
R16	$CH_3O_2 \rightarrow 0.330\ CH_3O + 0.335\ HCHO + 0.335\ CH_3OH$	$1.8\times10^{-13} \times e^{(416/T)} \times \sum RO_2$	$7.4\times10^{-13} \times \sum RO_2$
R17	$C_2H_5O_2 \rightarrow 0.6\ C_2H_5O + 0.2\ CH_3CHO + 0.2\ C_2H_5OH$	$3.1\times10^{-13} \times \sum RO_2$	$3.1\times10^{-13} \times \sum RO_2$

[*] Rate constant expressions are from the Master Chemical Mechanism (MCM),(Jenkin et al., 1997; Saunders et al., 2003) version 3.3.1, except R7 and R9, which are from Kabir et al. (2014)

** calculated using $[O_2] = 4.2\times10^{18}$ molecules cm^{-3}

Table 4: Arrhenius parameters for thermal dissociation of selected PN, PAN, PPN, PAA, and O_3.

Molecule	A (s^{-1})	E_a (kJ mol^{-1})	Reference	T needed to dissociate 0.1% (°C)**	T needed to dissociate 99.9% (°C)**
HO_2NO_2 (PNA)	7.3×10^{14} *	88.1±4.4	(Atkinson et al., 1997)	24	123
$CH_3O_2NO_2$ (MPN)	1.1×10^{16}	88.1±4.4	(Atkinson et al., 1997)	3	86
$C_2H_5O_2NO_2$ (EPN)	8.8×10^{15}	86.5±8.7	(Atkinson et al., 1997)	0	82
$CH_3C(O)O_2NO_2$ (PAN)	2.8×10^{16}	113±2	(Kabir et al., 2014)	73	174
$C_2H_5C(O)O_2NO_2$ (PPN)	2.36×10^{16}	113±2	(Kabir et al., 2014)	75	176
$CH_3C(O)O_2H$ (PAA)	10^{14}	134±8	(Schmidt and Sehon, 1963)	206	377
$CH_3C(O)O_2H$ (PAA)	1.15×10^{13}	136	(Devush et al., 1983)	247	450
$CH_3C(O)O_2H$ (PAA)	5×10^{14}	168±4	(Sahetchian et al., 1992)	300	492
O_3	1.3×10^{10} *	92.8	(Jones and Davidson, 1962; Heimerl and Coffee, 1979)	180	433

* Calculated assuming a pressure of 550 Torr and temperature of 298 K.

** Assuming a contact time of 4 ms at the maximum temperature (Paul et al., 2009)

Table 5: Products of CL and F for PNA and PAN at 110 °C, 80 °C, and 60 °C (RH = 34%)

	$\text{CL}_{110\,°\text{C}} \times \text{F}_{110\,°\text{C}}$	$\text{CL}_{80\,°\text{C}} \times \text{F}_{80\,°\text{C}}$	$\text{CL}_{60\,°\text{C}} \times \text{F}_{60\,°\text{C}}$
PNA	41.8 ± 0.2	39.5 ± 0.2	31.9 ± 0.1
ΣPAN	10 ± 1	7.6 ± 0.9	1.2 ± 0.2

Table 6: Statistics (average ± 1 standard deviation) of the 1 s data shown in Figure 12.

	PNA (pptv)			PAN (pptv)		
Time period	T1 = 110 °C T2 = 60 °C	T1 = 110 °C T2 = 80 °C	T1 = 80 °C T2 = 60 °C	T1 = 110 °C T2 = 60 °C	T1 = 110 °C T2 = 80 °C	T1 = 80 °C T2 = 60 °C
21:48:45 – 21:49:15	266 ± 4	254 ± 17	267 ± 4	447 ± 26	495 ± 75	430 ± 31
21:51:15 – 21:52:45	261 ± 5	258 ± 14	261 ± 6	480 ± 32	491 ± 68	476 ± 38

Table 7: Statistics (average ± 1 standard deviation) of the 1 s data of laboratory air (first time period), laboratory air spiked with ~260 pptv PNA (second period), and laboratory air spiked with 260 pptv PNA and ~480 pptv PAN (third period). n/a = not applicable.

	ΣPN (ppbv)			ΣPAN (ppbv)		
Time period	T1 = 110 °C T2 = 60 °C	T1 = 110 °C T2 = 80 °C	T1 = 80 °C T2 = 60 °C	T1 = 110 °C T2 = 60 °C	T1 = 110 °C T2 = 80 °C	T1 = 80 °C T2 = 60 °C
Room air	-0.08 ± 0.01	-0.29 ± 0.03	-0.068 ± 0.004	4.21 ± 0.04	5.1 ± 0.1	3.89 ± 0.03
Room air + PNA	0.19 ± 0.01	-0.03 ± 0.02	0.20 ± 0.01	3.50 ± 0.03	4.4 ± 0.1	3.17 ± 0.04
Δ(ΣPN)	0.27 ± 0.01	0.26 ± 0.04	0.27 ± 0.01	n/a	n/a	n/a
Room air + PNA + PAN	0.19 ± 0.01	-0.02 ± 0.02	0.20 ± 0.01	3.99 ± 0.04	4.8 ± 0.1	3.70 ± 0.03
Δ(ΣPAN)	n/a	n/a	n/a	0.49± 0.04	0.40 ± 0.14	0.52 ± 0.05

Figures

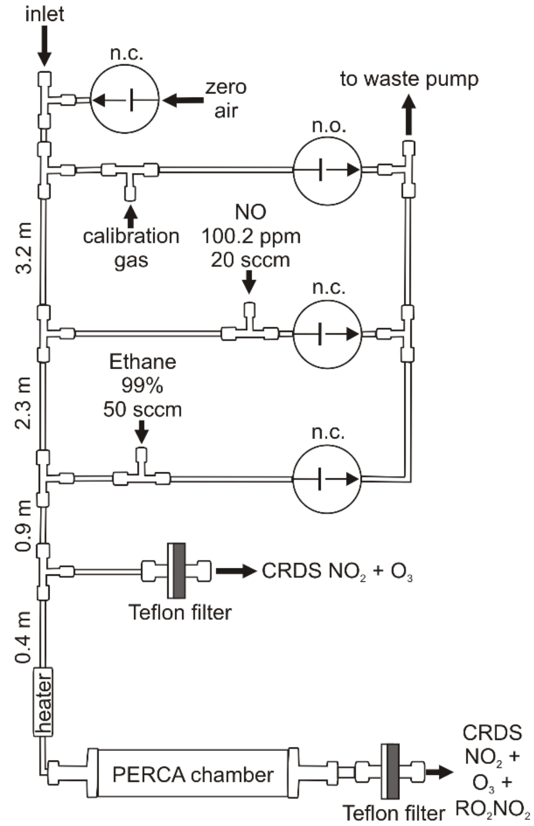

Figure 1. Schematic of the dual-channel thermal decomposition peroxy radical chemical amplification inlet. The inlet consists of a 60 cm long, 0.635 cm (¼") o.d. quartz heater and an 80 cm long, 1.27 cm (½") o.d. FEP Teflon™ reaction chamber. Reaction gases were added upstream of the PERCA chamber by closing the normally open valves connected to a waste pump via 50 µm critical orifices. Background NO_2 levels were monitored in a parallel detection channel by tapping into the inlet prior to thermal dissociation of peroxy nitrates.

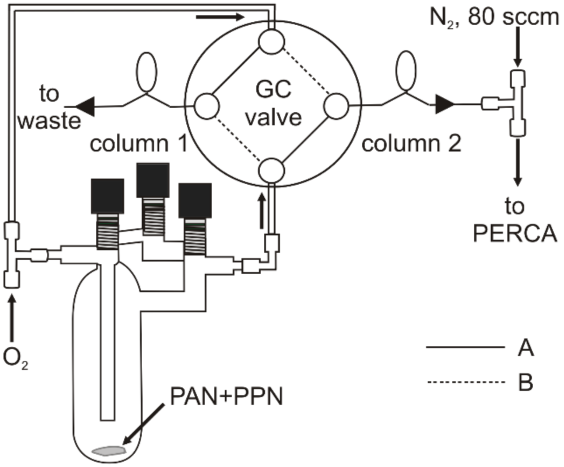

Figure 2. Setup for delivery of PAN and PPN using a gas chromatography column.

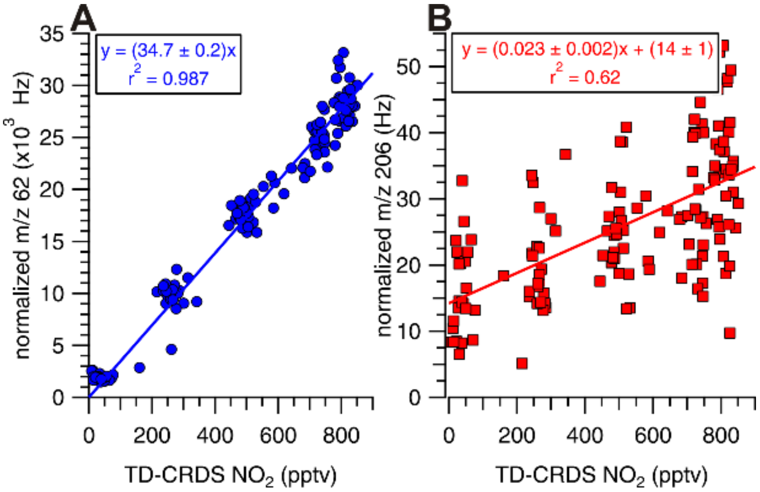

865

Figure 3. Calibration of CIMS response factors against TD-CRDS operated with its inlet heated to 120 °C and without amplification. (A) *m/z* 62. (B) *m/z* 206. CIMS counts were normalized to 10^6 I^- counts.

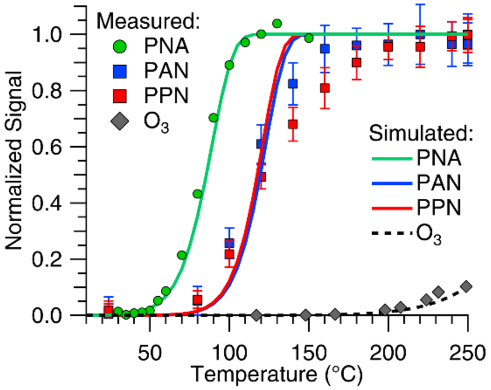

Figure 4. Normalized thermal dissociation profiles of PNA, PAN, PPN, and O_3 as a function of inlet set temperature. Superimposed trend lines are simulations based on the TD model introduced by Paul et al. (2009). The PNA, PAN, and PPN data were observed by TD-CRDS without amplification gases present, whereas the O_3 data were observed by TD-PERCA-CRDS. The error bars represent standard deviations of 1 s data.

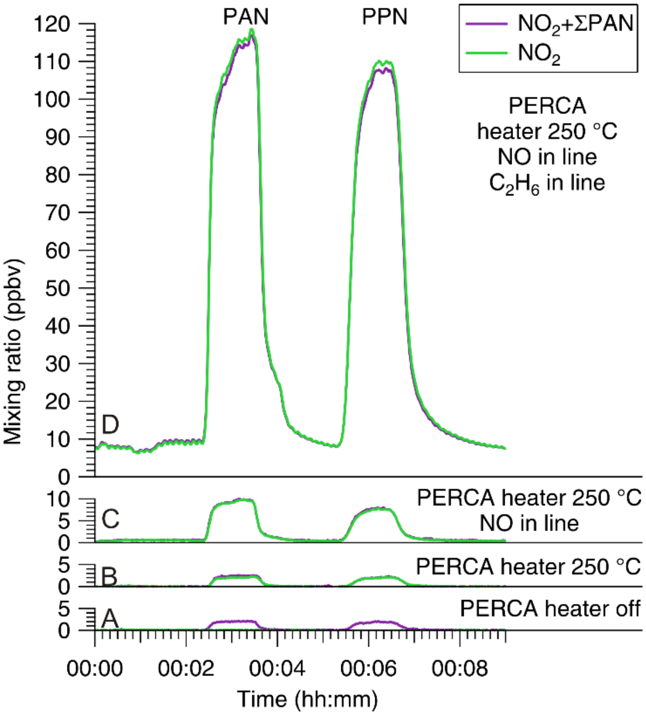

Figure 5. Peroxy radical chemical amplification of peroxyacetic and peroxypropionic nitric anhydride (PAN and PPN) delivered via a megabore GC column. (A) Time series of the signal observed by cavity ring-down spectroscopy in the ambient temperature (NO_2; green colour) and heated (NO_2 + ΣPAN; purple colour) channels with the PERCA heater off. (B) Same as (A) with the PERCA heater switched on. (C) Same as (B) with 0.75 ppmv NO added. (D) Same as (C) with 1.5% C_2H_6 added. The amplification factor is determined from the ratio of the ambient temperature (i.e., NO_2) CRDS signal observed in (D) divided by that observed in (B).

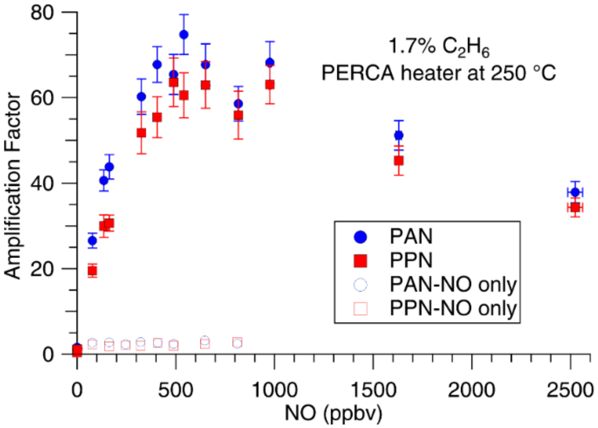

890 **Figure 6. TD-PERCA-CRDS amplification factors of ~0.5 ppbv PAN and ~1.3 ppbv PPN as a function of NO mixing ratio at RH = 0%. The error bars represent standard deviations of 1 s data.**

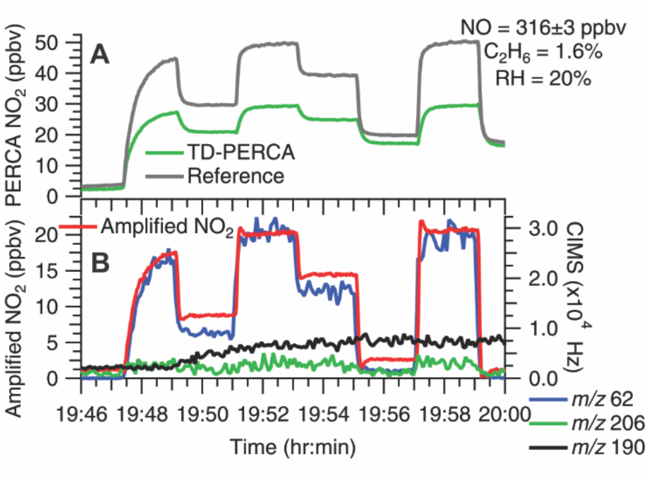

Figure 7. (A) Sample time series of PNA observed by TD-PERCA-CRDS in the reference, NO_2 channel (shown in green) and PERCA channel (grey). (B) (left) Difference signal between amplified and reference channel (shown in red). (right) CIMS counts (normalized to 10^6 I^-) at *m/z* 62, the major fragment (NO_3^-) expected from PNA, at *m/z* 206 (multiplied by a factor of 100 for clarity), the $HNO_4{\cdot}I^-$ cluster, and at m/z 190, the $HNO_3{\cdot}I^-$ cluster.

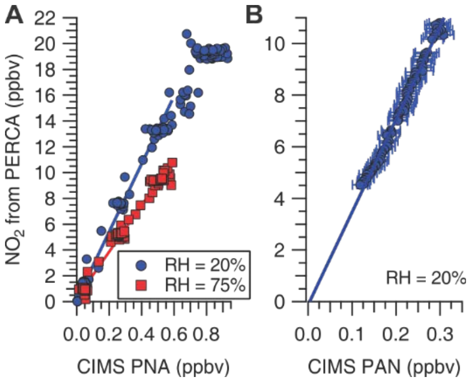

Figure 8. Scatter plots of TD-PERCA-CRDS and CIMS measurements. (A) Sample PNA calibrations at an NO mixing ratio of 316±3 ppbv and TD-PERCA inlet temperature of 120 °C. For mixing ratios <0.6 ppbv, the intercept and slope of the linear fits are (0.2±0.1) ppbv and 26.3±0.4 (r^2 = 0.979) at RH = 20% and (0.3±0.1) ppbv and 18.0±0.2 (r^2 = 0.985) at RH = 75%. (B) Sample PAN calibration at an NO mixing ratio of 662±2 ppbv and TD-PERCA inlet temperature of 250 °C and RH = 20%. The intercept and slope of the linear fit is (-0.13±0.09) ppbv and 36.0±0.4 (r^2 = 0.990).

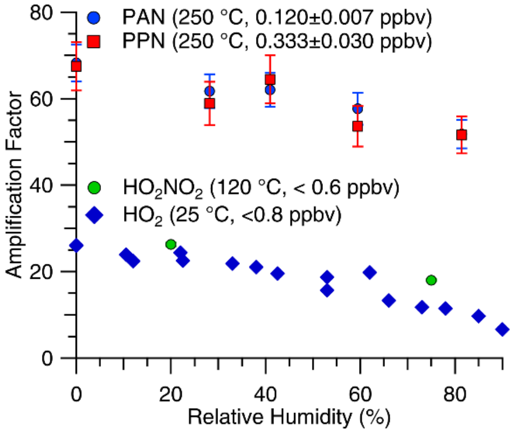

Figure 9. TD-PERCA-CRDS amplification factor as a function of relative humidity at an ethane mixing ratio of 1.6% and with NO mixing ratios of 644±2 and 316±3 ppbv for the PAN/PPN experiments and the PNA experiments, respectively. The PAN and PPN mixing ratios were 0.120±0.007 and 0.333±0.030 ppbv, respectively. The PNA mixing ratio was varied between 0 and 0.6 ppbv. The room temperature HO_2 data are from Wood et al. (2016).

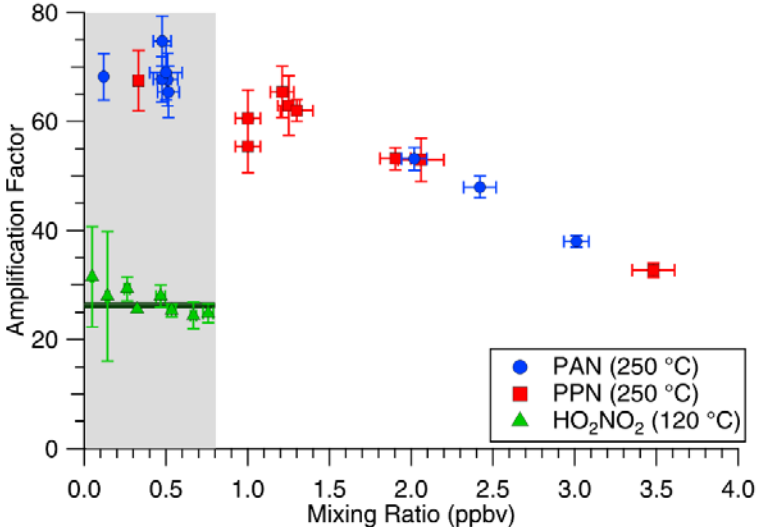

Figure 10. TD-PERCA-CRDS amplification factors as a function of PAN, PPN, and PNA mixing ratio. Errors bars correspond to ±1σ standard deviation. Mixing ratios of NO and ethane were 500±50 ppbv and ~1.6%, respectively. The grey underlay indicates the linear range. The dark green line corresponds to 26.3±0.4 (slope of data shown in Figure 8A).

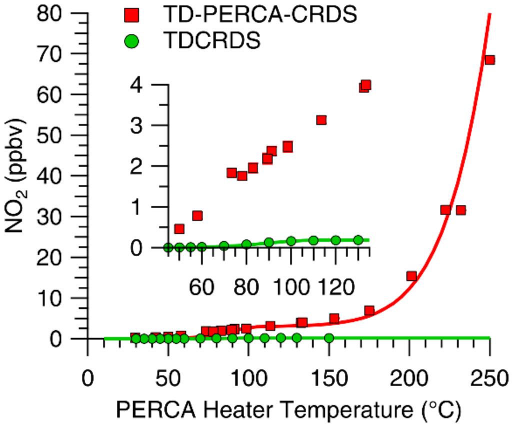

Figure 11. Amplification of photochemically generated PNA (red) as a function of PERCA heater temperature (RH=24%). Simultaneous quantification by CIMS and UV absorption showed that the gas stream contained 180±28 pptv PNA and 3.5±0.2 ppbv O$_3$. The non-amplified TD-CRDS signal (from Figure 4), multiplied by 0.18, is shown in green for comparison.

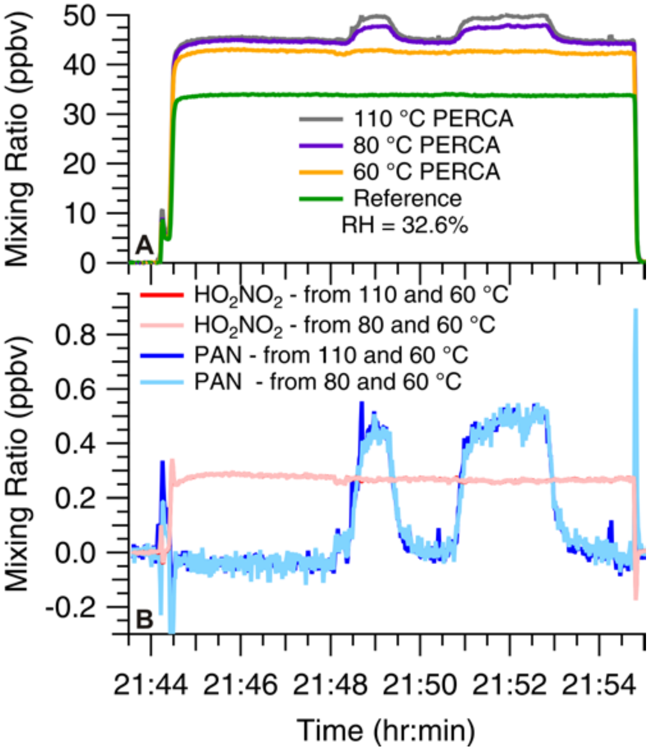

Figure 12. Demonstration of differential temperature TD-PERCA-CRDS. (A) Time series of NO_2 mixing ratios observed by an unheated reference channel and three TD-PERCA channels operated at 60 °C, 80 °C, and 110 °C, respectively. PNA was sampled from 21:44:30 to 21:54:45, and PAN was added at ~21:49 and ~21:52. (B) Mixing ratios of PAN and PNA calculated from (A).